Night Vision and Electronic Sensors Directorate

AMSEL-NV-TR-0118

The Influence of Focal Plane Array Design Parameters on Future Automatic Target Recognizer Performance

by

Daniel Goodman, Hanna Tran, Brian DeCamp, James D. Howe, Timothy Williams, Joan Kruthers, Gary O'Brien, Kristina Le, and Jae Cha

May 1995

FORT BELVOIR, VIRGINIA 22060-5806

Destroy this report when it is no longer needed.
Do not return it to the originator.

The citation in this report of trade names of commercially available products does not constitute official endorsement or approval of the use of such products.

REPORT DOCUMENTATION PAGE

Form Approved
OMB No. 0704-0188

1. AGENCY USE ONLY *(Leave blank)*	2. REPORT DATE	3. REPORT TYPE AND DATES COVERED
	May 1995	Final 1 Dec 1991 to 30 Nov 1992

4. TITLE AND SUBTITLE

The Influence of Focal Plane Array Design Parameters on Future Automatic Target Recognizer Performance (U)

5. FUNDING NUMBERS

6. AUTHOR(S)

Daniel Goodman, Hanna Tran, Brian DeCamp, James D. Howe, Timothy Williams, Joan Kruthers, Gary O'Brien, Kristina Le, and Jae Cha

7. PERFORMING ORGANIZATION NAME(S) AND ADDRESS(ES)

Night Vision & Electronic Sensors Directorate
10221 Burbeck Road, Suite 430
ATTN: AMSEL-RD-NV-AOD-SMT
Fort Belvoir, Virginia 22060-5806

8. PERFORMING ORGANIZATION REPORT NUMBER

AMSEL-NV-TR-0118

9. SPONSORING/MONITORING AGENCY NAME(S) AND ADDRESS(ES)

10. SPONSORING/MONITORING AGENCY REPORT NUMBER

11. SUPPLEMENTARY NOTES

POC: Timothy J. Williams, (703) 704 1685

12a. DISTRIBUTION/AVAILABILITY STATEMENT

Approved for public release; distribution unlimited.

12b. DISTRIBUTION CODE

13. ABSTRACT *(Maximum 200 words)*

Automatic cuers and recognizers have been included in many recent weapons systems designs. In systems such as the Comanche helicopter a successful cuer/recognizer will significantly reduce crew workloads and will shorten acquisition timelines considerably. Focal plane array development has matured to the point where a new generation of common detector modules are being built under the IRFPA program. In the initial phases of the program it became important to take a look at different proposed array configurations, and to try to draw conclusions about the resulting image quality and impact that would have on future automatic target recognizer performance.

The focus of this investigation has been the impact of several key FPA parameters on ATR performance. The experimental design was chosen to be independent of specific ATR algorithms and focused on the amount of image degradation and information loss attributable to a particular FPA design change. Sensor parameters studied included detector size, detector geometry, noise, detector response nonuniformity, and array sampling effects. Range dependence of the image quality degradation due to each of the sensor parameters is presented.

14. SUBJECT TERMS	15. NUMBER OF PAGES
forward looking infrared focal plane array, Automatic Target Recognizer, sampling rate, detector geometry, detector non-uniformity, interlace effects, signal to noise ratio (SNR)	76
	16. PRICE CODE

17. SECURITY CLASSIFICATION OF REPORT	18. SECURITY CLASSIFICATION OF THIS PAGE	19. SECURITY CLASSIFICATION OF ABSTRACT	20. LIMITATION OF ABSTRACT
Unclassified	Unclassified	Unclassified	UL

NSN 7540-01-280-5500

Standard Form 298 (Rev. 2-89)
Prescribed by ANSI Std. Z39-18
298-102

Report Number 0118

The Influence of Focal Plane Array Design Parameters on Future Automatic Target Recognizer Performance

by

Daniel Goodman, Hanna Tran, Brian DeCamp, James D. Howe, Timothy Williams, Joan Kruthers, Gary O'Brien, Kristina Le, and Jae Cha

Night Vision and Electronic Sensors Directorate
Fort Belvoir, Virginia 22060-5806

Accesion For	
NTIS CRA&I	☒
DTIC TAB	☐
Unannounced	☐
Justification	
By	
Distribution /	
Availability Codes	
Dist	Avail and / or Special
A-1	

May 1995

Table of Contents

LIST OF FIGURES

Page

Page

LIST OF TABLES

Acknowledgements

The authors would like to thank Jim Hilger, Paul Brewer, and Scott Tran for their work in writing software and generating data simulating horizontal and vertical interlace misregistration for this study.

Section 1 Summary

The influence of parallel scanned focal plane array (FPA) design parameters on future automatic target recognizer (ATR) performance was examined. The design variables tested were instantaneous field of view (IFOV) size and shape, sampling rate, sample-scene phasing effects, signal to noise ratio (SNR), residual detector-to-detector nonuniformity and interlace effects. Simulated forward looking infrared system (FLIR) designs for this experiment were chosen to span design choices similar to typical "first" and "second generation" tactical Army FLIRs.

The influence of field misregistration due to the interaction of jitter and interlaced scanning was investigated first using a statistical classifier as the ATR. Misregistration of fields by one or two pixels was shown to degrade classification performance significantly. The influence of interlace on three different types of trackers was also examined. Interlace was shown to either seriously degrade tracker performance or cause the tracker to completely break lock.

In an effort to make the results of the testing applicable to a large class of algorithms and not be algorithm specific a more general approach was taken. A high resolution reference image was correlated with the same image after having been passed through a simulated atmosphere and FLIR. The degraded image was systematically shifted with respect to the starting image and a correlation surface was calculated, the peak of which was used as a measure of future algorithm performance.

In the absence of atmospheric effects, the noise values chosen for this experiment did not degrade correlation significantly since the signal from target and background was so large relative to the noise. Almost all correlation degradation with range was caused by blurring due to optics, detector and the sampling process.

The simulated atmospheres by themselves, while seriously degrading the contrast in the image, had very little effect on correlation peak values. However, when noise and atmospheric effects were simulated together, they drastically degraded the signal to noise in the image, and the correlation peak values were significantly reduced to the point where the image would not be usable for automatic target recognition.

Of the three values for nonuniformity examined, only the largest was seen to seriously degrade correlation when examined alone. As with the noise case, combining the influence of nonuniformity and atmosphere drastically degraded correlation values.

Increasing the sampling rates while holding other variables constant improved performance, as would be expected. The correlation peak value for 1.5 samples per dwell (spd) was equivalent to the correlation peak for a similar system with 1.0 spd at 1000 meters shorter range. That is, the same quality image was obtained at greater range with the higher sampling rate. Similarly, the correlation values for 2.0 spd were equal to those for 1.5 spd at approximately 500 meters closer range. These trends held for all ranges tested (3 - 6 km) and for both square and rectangular detectors.

Correlation was shown to be strongly influenced by the number of samples on target up to approximately 500 samples / mrad2. This is consistent with past observations that algorithm performance is a strong function of the number of pixels on target.

Larger detectors degraded the system resolution and thus the correlation values. However, if the system was assumed to be BLIP limited with larger detectors resulting in less noise in the final image, the larger detectors were shown to have advantages in low SNR conditions.

Sample-scene phasing causes variation of the target appearance for slightly different alignments of a FLIR line of sight (LOS). The effect is most pronounced for the lowest sample rate tested, 1 spd, and is most prominent when the image is improperly reconstructed. The effect is strongly range dependent, being most noticeable at longer ranges. For 2 spd and good reconstruction the effect is negligible, even at long ranges, as would be expected. Minimizing the variation of the appearance of the target with changing LOS will decrease the frame to frame variation in algorithm performance, thus increasing robustness. This robustness afforded by the high sampling rates, especially at the longer ranges is a good reason to push FPA designs toward higher sampling rates. This phasing effect has not been explored in previous efforts.

Preliminary investigations of image restoration show promise. We will continue to investigate the benefits of restoration of simulated and real FLIR imagery.

Section 2 Introduction

The overall performance of a thermal imager, whether designed to produce an image for a human or an autoprocessor, depends critically upon the design and performance of the focal plane array (FPA). As the U. S. begins the design and construction of a second generation of infrared FPAs it is important to investigate the influence of various array designs, not only on the human, the traditional end user of the IR image, but, equally as important, on autoprocessors which are taken here to include trackers, autocuers and automatic target recognizers.

First generation FLIR systems currently in the Army inventory produce imagery with numerous artifacts such as streaking caused by AC coupling, and jagged edges caused by imperfect interlace. The artifacts often produce dramatic variations in the appearance of a target from frame to frame. To a human observer whose eyes integrate a displayed image for approximately 0.2 seconds (or about 6 frames) such variation may be noticed only as a slight blurring of the imagery. However, to a target recognizer which operates on every frame of imagery, the frame to frame variation can be disastrous. Figure 1 shows the result of a statistical classifier operating on a consecutive sequence of 60 first generation FLIR images of a stationary target. The target has been segmented in each image by the algorithm and the target's height-to-width ratio has been measured. This ratio is one of several which are used by the algorithm to discriminate between different target types. It is easy to see how the frame to frame instability of the first generation imager could cause drastic variations in algorithm performance.

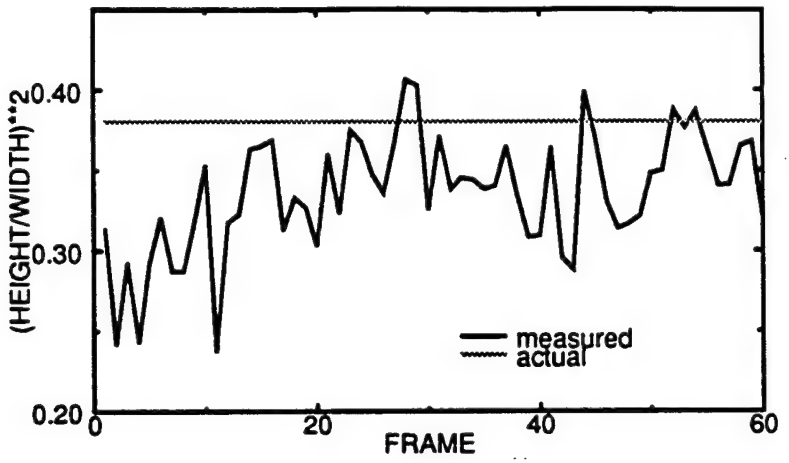

Figure 1. Frame to frame variations of the (height/width)^2 ratio for 60 consecutive frames of first generation FLIR imagery

The FPA candidates which were thought to best address U. S. Army weapon system applications were parallel scanning FPAs of different lengths and architectures. Critical FPA design issues involved parameters which not only strongly impacted system performance but, at the same time,

directly influenced FPA producibility and cost. Those FPA design parameters which were identified as being crucial to both system performance and FPA producibility were the following.

1. Interlaced vs. noninterlaced image format.

2. Sample spacing in both scan and orthoscan directions.

3. Signal to noise (SNR), including nonuniformity.

4. Detector size and geometry (rectangular vs. square).

The goal of this study was to quantify the effects of these parameters on algorithm performance separately so that cost/performance trade-offs could be made. Ideally this study should be designed to determine the effects of these parameters on the next generation of autoprocessors. The focus of current algorithm research is shifting from statistical classifiers to template matching or model based algorithms. These future algorithms could have totally different sensitivities to FPA designs than statistical classifiers, and we should not be designing tomorrow's FPA for use with yesterday's algorithm. Yet, without tomorrow's algorithms in hand, it is difficult to perform testing which properly indicates the sensitivities of future algorithms to various FPA designs.

This study began with an investigation of the influence of interlace artifacts on the performance of a statistical classifier. The use of a single algorithm to explore sensitivities of a class of future algorithms to interlace ran into technical difficulties to be explained in detail later in this report. The results were thought to be too algorithm specific as alluded to above. After the examination of interlace issues using a statistical classifier, a more general approach was chosen to examine sampling, SNR, detector size/shape, nonuniformity, and also to reexamine interlace.

While the study was directed at examination of FPA parameters, it could not be carried out without choosing a FLIR system design or set of designs. FPA designs must be examined while considering the array as a component of a FLIR system. The optimal FPA will be a function of many other FLIR system components.

The portion of the study which dealt with the influence of interlace using a statistical classifier is dealt with separately in Section 3 since the approach was different from the rest of the study. Section 4 covers the influence of sampling, S/N and detector size/shape, and looks again at interlace. Section 6 summarizes work on a companion project dealing with the influence of interlace misregistration on trackers. Conclusions are presented in Section 7.

Section 3 Influence of Interlace on a Statistical Classifier

3.1 IMAGERY DISTORTIONS RELATED TO INTERLACE

Figure 2 illustrates three different interlace mechanisms which contribute to distortion of target shape within a single frame which is composed of two interlaced fields. They are due to a bidirectional parallel scan mechanism, a unidirectional parallel scan and a staring array with odd and even field readout separated by 1/2 the total frame time. Other interlace configurations such as serial-parallel are possible but are not candidates for second generation FPAs and, therefore, are not considered here.

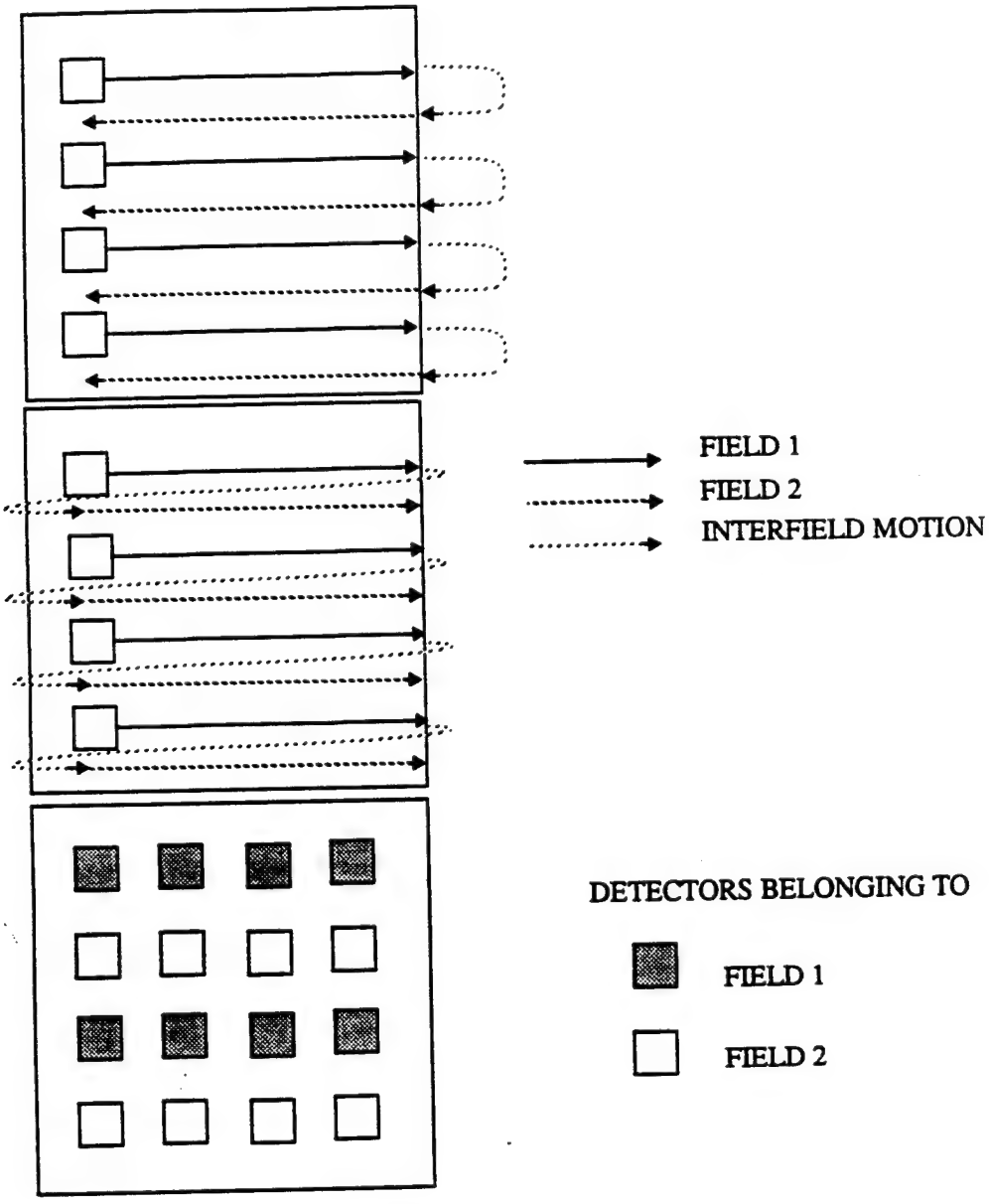

Figure 2. Motion of the image across a) a bidirectionally interlaced FPA, b) a unidirectionally interlaced array and c) an interlaced staring array

In order to understand the reasons for distortion of a target due to interlacing it is important to consider the time interval between different fields of a single frame of imagery. For an interlaced staring sensor the even fields integrate signal for 1/60 of a second and then read out, after which the odd fields integrate and read signal out. Any translation or rotation of the line of sight (LOS) of the FLIR (this includes jitter), misregistration of the scan mechanism, or motion of the target during the interval between fields will shift the target image in one field relative to the other. When the fields are combined into a single frame, a distortion of the target will result. The final form of the distortion will depend upon the direction of motion of one field with respect to the other.

If there were any jitter in the LOS after correction by gimbals and fine stabilization mechanism, the interaction of the residual jitter and the interlace could combine to produce target distortions. For example, if jitter moves the sensor LOS up toward the end of the scan of field 1, as is shown in Figure 3, the edges of the target which do not lie parallel to the direction of motion will become jagged and the aspect ratio of targets will change as will the square in the figure. If the jitter were to move the LOS along the direction of scan, as in Figure 4, again the edges of targets would become distorted. This is the same type of distortion which would result if a tactical target were travelling rapidly parallel to scan. This same type of shearing would be apparent if the velocity of the scene presented to an interlaced imager was large, as is the case when the FLIR LOS is directed perpendicular to the platform velocity. This would be the case when a pilot steers a head-slaved FLIR perpendicular to the line of motion in a low flying aircraft.

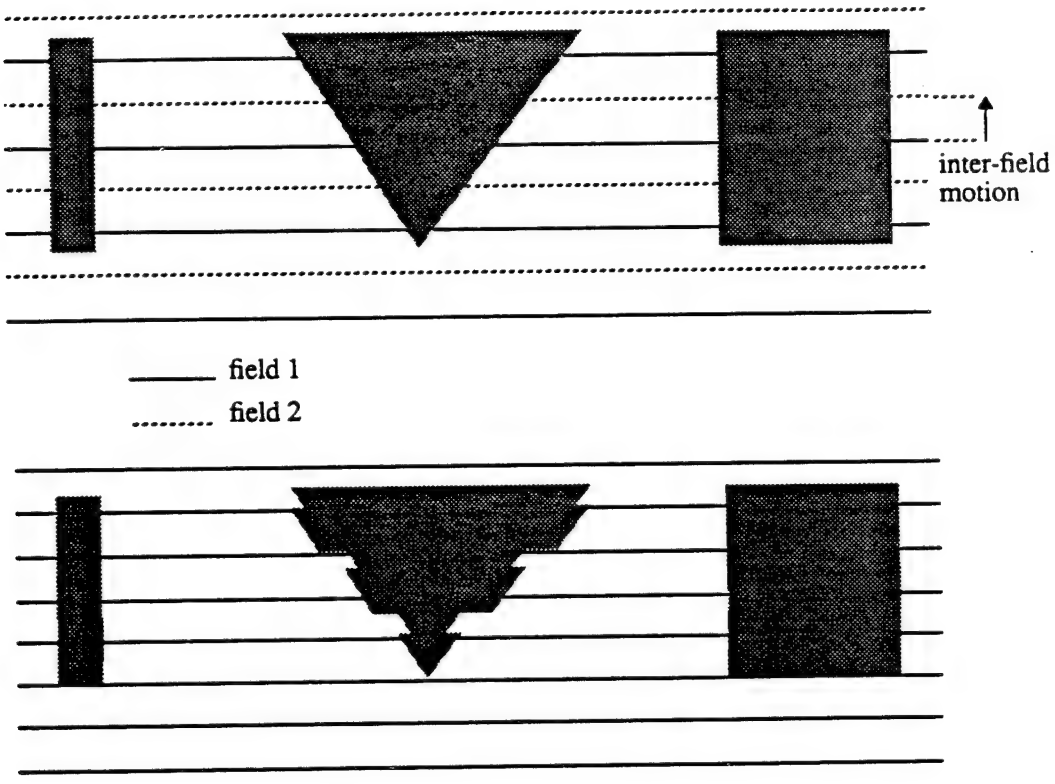

Figure 3. Distortions caused by a simple vertical motion of the LOS between field 1 (solid) and field 2 (dashed). b) The resulting frame showing jagged edges and aspect ratio variation

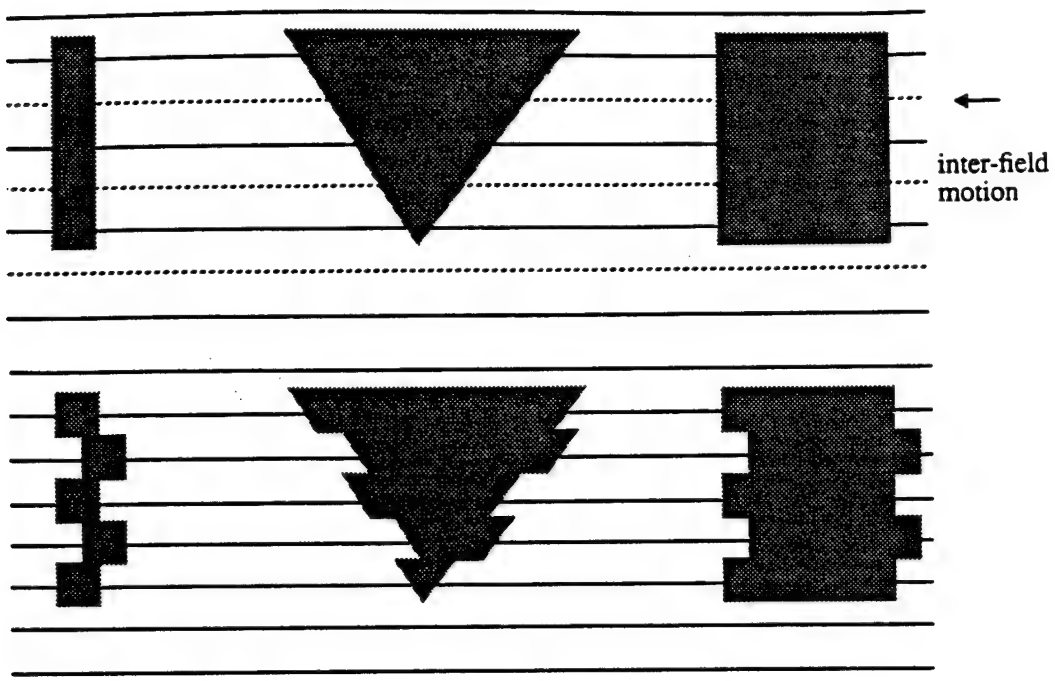

Figure 4. Distortions caused by a simple horizontal motion of the LOS between field 1 (solid) and field 2 (dashed). b) The resulting frame showing jagged edges and aspect ratio variation

For bidirectionally scanned arrays (Figure 2a) the time interval between scanning across an edge of a target in one field and stepping down and scanning back across the same edge will depend upon the position in the field of view. The distortions within a frame will therefore be dependent upon their position in the field of view.

Naturally, the actual distortions will be more complicated than those mentioned above, being a complex function of the scan velocity and frequency spectrum of the residual jitter. Residual high frequency jitter will act to displace the system LOS within a field. For a staring system which integrates for a frame time, this will result in a blurring. For a parallel scanning system the different displacements of the LOS along a scan will produce waves, stretches, and warping along the scan line. The two types of jitter described in Figure 3 and Figure 4 will serve as paradigms of simple distortion with which we will probe the magnitude of the interlace effects on algorithm performance.

Distortions of a target when measured in pixels will be a greater percentage of total target subtense at greater ranges. Thus, even distortions which are sometimes thought to be small (those on the order of just a few pixels), become increasingly important at longer ranges.

3.2 HORIZONTAL MISREGISTRATION OF INTERLACED FIELDS

The imagery used in this experiment consisted of terrain board imagery of 21 aspects of two vehicles, an M35 truck and an M1 tank, at simulated ranges of 3500 and 4500 meters.[1] Horizontal misregistration of interlaced fields was simulated by shifting all odd lines in each image, corresponding to the distortions illustrated in Figure 4. Five sets of shifted images corresponding to pixel shifts of 0.5, 1.0, 1.5, 2.0, 2.5 were created in this manner. Together with the unshifted imagery this resulted in a total of 504 images.

The Hughes ADASIM algorithm was then used to segment the targets from the imagery and extract a set of 20 features from each segmentation.[2,3] Examples of the unshifted, shifted and segmented imagery are shown in Figure 5. The features were then compared and analyzed in different ways; only the most productive procedures will be described here.

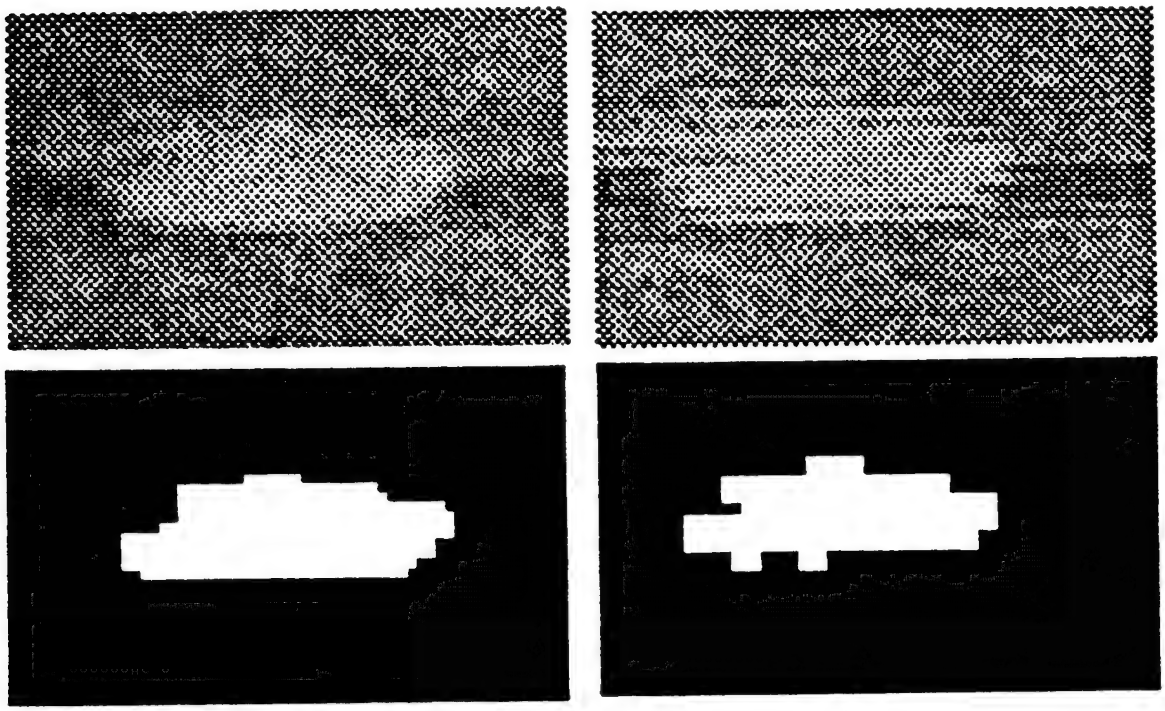

Figure 5. Examples of unshifted, shifted, and segmented images used in the experiment.

The percent change in feature value between nonshifted and shifted images averaged over all 21 aspects was examined. Target features changed as a result of the pixel shifting, but in no specific pattern. There was no gradual increase or decrease in the target feature values from non-shifted to shifted images.

The spread in feature value due to vehicle aspect was also examined versus pixel shift as show in Figure 6. In most cases the spread in feature value due to vehicle aspect was greater than the variation in feature value due to pixel shift. Although this result appears to indicate that the influence of pixel shifting was small, the comparison could be misleading if extrapolated to final performance of the algorithm. Target classification decisions are made using all 20 features, not

just a single feature, and because of this the appropriate comparison should be made in 20 dimensional feature space.

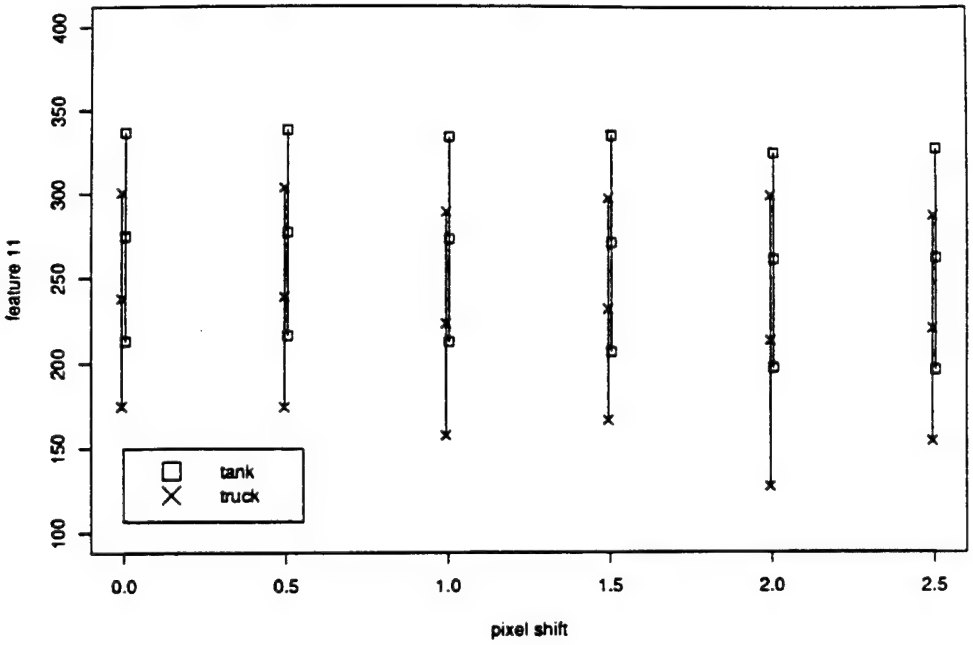

Figure 6. Variation of feature value (largest and smallest values and mean) for the truck and tank versus pixel shift

Due to the difficulty of illustrating results in a 20 dimensional space, the Bhattacharyya distance[4] was measured between feature values which had been averaged over aspect. The Bhattacharyya distance is a measure on Euclidean n-dimensional space. For uncorrelated features the Bhattacharyya distance can be thought of as a result of a change of coordinates: the origin of n-space is translated to the vector whose i^{th} component is the mean of the i^{th} feature, and the i^{th} coordinate axis has its scale given by the standard deviation of the distribution of the ith feature. Those features between which there was the greatest distance were assumed to be the best target discriminators. The top three features for each range were determined in this manner, and feature values for each aspect of the tank and truck were plotted in the three dimensional space having those features which were identified to be the best discriminators as dimensions in order to look for trends.

Figure 7 and Figure 8 show examples of the results for integer pixel shifts. One might expect the interlace to move the distribution systematically. Overlaying the shifted and nonshifted results does not appear to show any systematic motion or distortion of the distribution. Thus from this experiment we are unable to quantify the performance degradation due to different amounts of interlace misregistration.

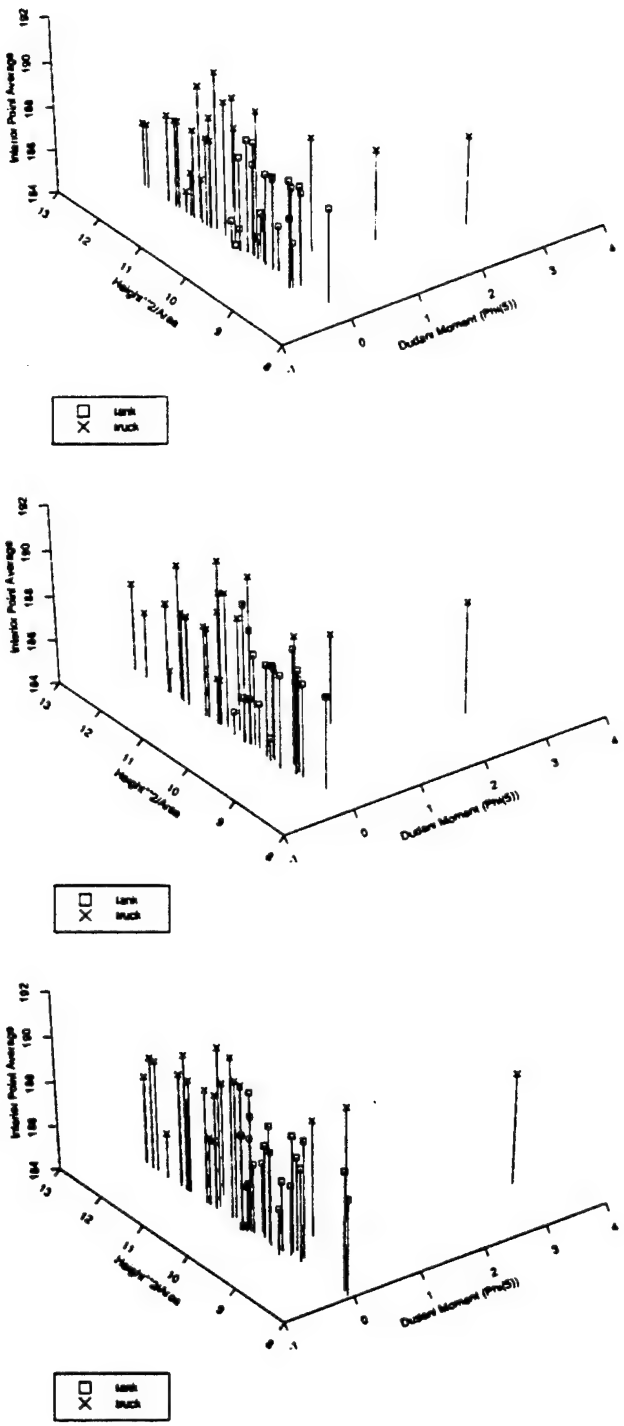

Figure 7. Three dimensional feature space representation of 21 different aspects of the tank and truck at 3500 meters for no pixel shift (top), **one pixel shift** (middle) **and two pixel shift** (bottom)

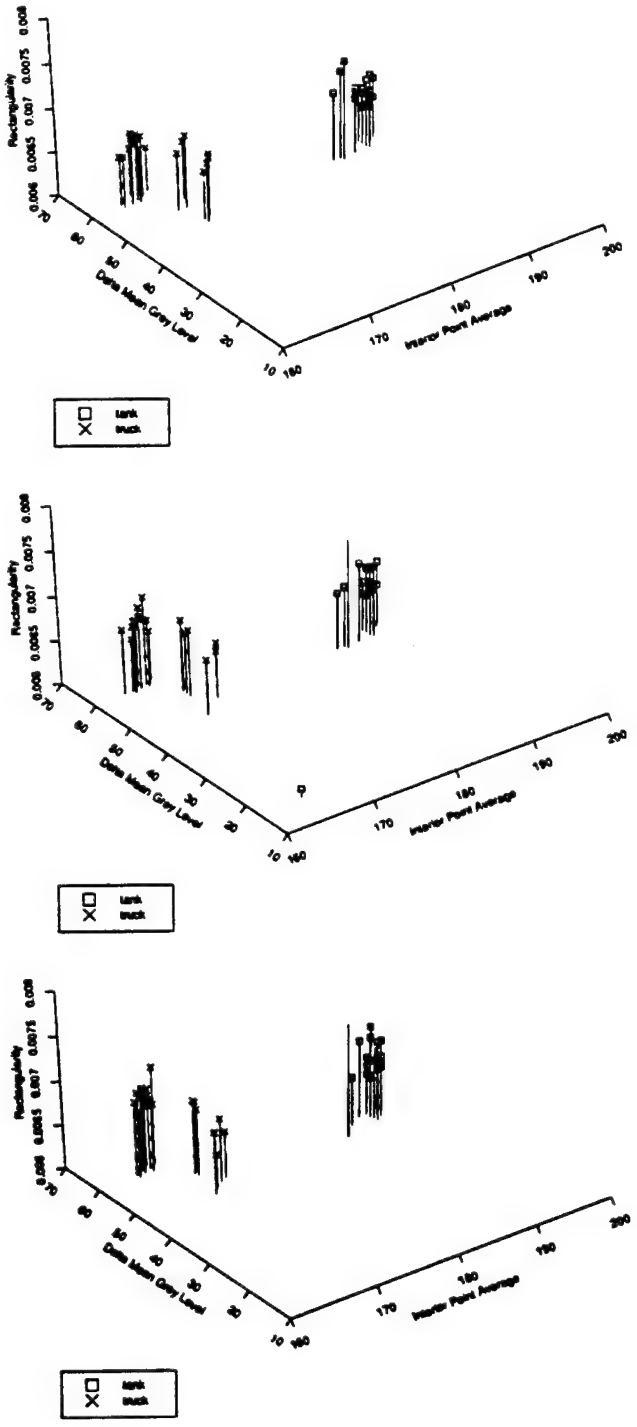

Figure 8. Three dimensional feature space representation of 21 different aspects of the tank and truck at 4500 meters for no pixel shift (top), one pixel shift (middle) and two pixel shift (bottom)

Since the approach using feature values ran into difficulties, we changed our approach and turned our attention to the final decision of the algorithm. The algorithm used a binary decision tree for final classification of the target. The shifting of fields due to interlace could possibly alter the final decision of the classifier. Variation of a feature value due to interlace above or below a specified threshold would alter the path followed along the decision tree. There are 124 terminal nodes on the decision tree, 24 of which classify the target as a tank. Since many of the terminal nodes of the decision tree can result in the same decision, an alteration in path down the tree caused by field shifting can result in either 1) the target classification being the same as the non-shifted classification (path b in Figure 9) or 2) the target classification being different (path c in Figure 9).

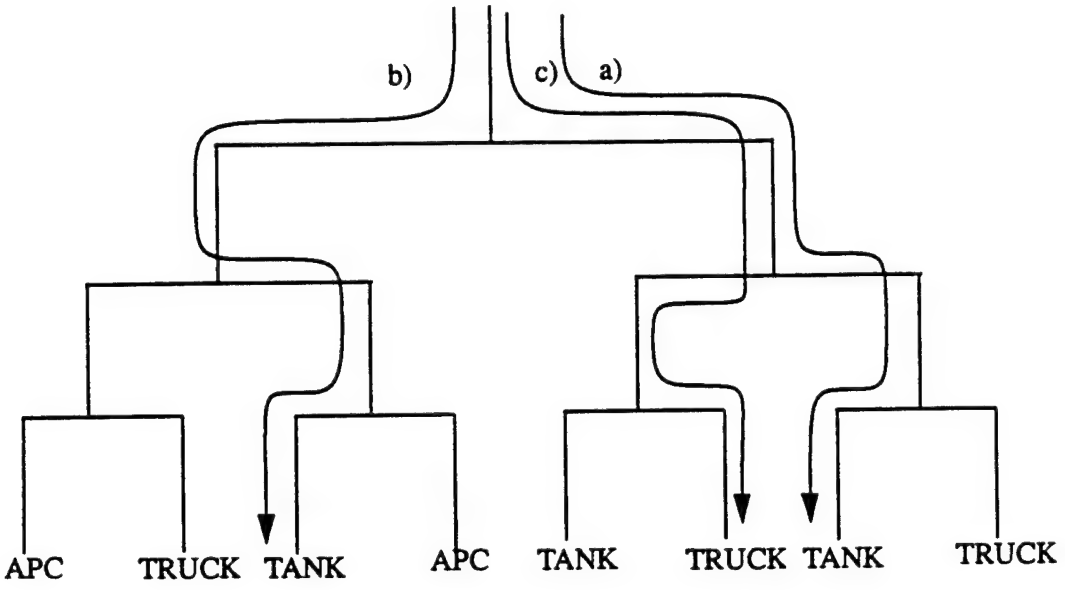

a) unshifted
b), c) possible shifted results

Figure 9. Possible paths taken down a decision tree. The solid line, labelled path a, could represent the path resulting from the noninterlaced image. Interlace could result in a path labelled path b which leads to the same classification at a different terminal node or a path labelled c which leads to a different classification.

The final classification of the shifted target can be the same as the nonshifted target in two ways: 1) by resulting in the same terminal node or 2) by resulting in a different terminal node with the same classification. We examined the percent of correct classifications at any terminal node (Table 1) and the percent of correct classifications at the same terminal node (Table 2).

Table 1. Percent of correct classifications at any terminal node

target	range	no shift	1.0 pixel shift	2.0 pixel shift
tank	3500m	90%	85%	86%
tank	4500m	90%	81%	76%

Table 2. Percent of correct classifications at the same terminal node as the unshifted image

target	range	1.0 pixel shift	2.0 pixel shift
tank	3500m	81%	76%
truck	3500m	76%	76%
tank	4500m	48%	52%
truck	4500m	57%	57%

One notices from Table 1 a pronounced influence of range. As one would expect, the distortions due to interlace become large relative to the size of the target at greater ranges, resulting in an increase in misclassifications. What we are not able to explain is the improvement in classification for the two pixel shift over the one pixel shift at 3000 meters. Table 2 indicates that there were changes in the path down the binary decision tree due to the simulated interlace misregistration. Also evident is the influence of range as in Table 1.

3.3 VERTICAL MISREGISTRATION OF INTERLACED FIELDS

A different approach was tried for the investigation of the influence of vertical scan misregistration due to interlace. The same set of images, 21 aspects of the two targets M1 and M35 at 3500 and 4500 meters, was used as a starting point for the testing. From each of the 84 images a set of 10 images was created by vertically shifting the odd field a random amount from 0.0 to 2.0 pixels. For noninteger shifts a linear interpolation between adjacent rows in the original image was used to determine the pixel value for the odd field.

The strategy for this segment of the testing was to measure the Bhattacharyya distance between the two classes of targets and use it to give an estimate of the upper bound on the probability of classification. Hughes ADASIM was used to generate features for calculating the Bhattacharyya distance. This statistical measure uses the mean feature vector and the covariance matrix of the features for each of the two target classes. The Bhattacharyya distance assumes a Gaussian distribution of features in feature space. The Gaussian distribution is also an assumption which is common to most statistical classifiers. Although this is not an accurate assumption, it is important that the assumptions made in the test method be the same as those in the family of algorithms under test in order that the test results reflect the performance of the general class of algorithms.

The class separability for a noninterlaced system was estimated by using the Bhattacharyya distance between the 21 aspects of the M1 and the 21 aspects of the M35. The separability for an interlaced system was estimated by calculating the Bhattacharyya distance between the distorted silhouettes of the 21 aspects of the M1 and the 21 aspects of the M35. Since it was not known how many samples of the distorted images were needed, the experiment was repeated using a larger number of samples each time.

The results of the experiment are given in Figure 10. The horizontal axis in the graph indicates the number of images used. The vertical axis shows the log10 of the probability of error estimated by the Bhattacharyya distance. The probability of error approaches the asymptotes drawn as dotted lines in Figure 10. The degradation in performance due to an interlaced system is

represented by the difference in the probability of error between the noninterlaced case and the asymptotes for each range.

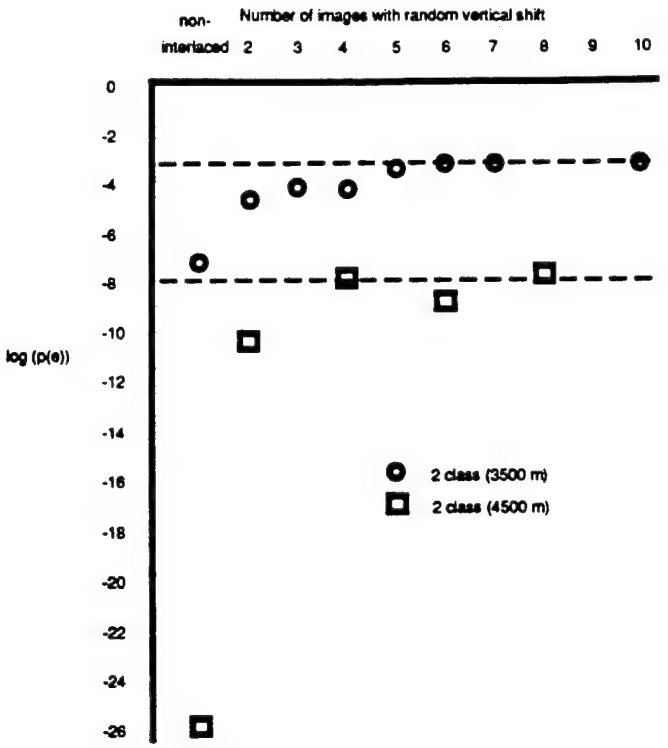

Figure 10. Results of the vertical misregistration test showing the log of the probability of error versus the number of images used to calculate the Bhattacharyya distance

The point at which the response curves approach the asymptotes represents the number of interlaced images (of each target at a specific aspect) required of future experiments. From Figure 10 it would seem that six to ten images with interlace distortion would produce about the same separability results as many thousands of images with the same distortion.

The first thing that one notices about the results is that the final probability of error is estimated to be very small. It is thought that this is the case because of the very small target set. In order to get more realistic probabilities of error, it would be necessary to run the experiment on a larger data set size.

Another unexpected result of this testing is that the separability increases for the longer range targets. Intuitively we know that at longer ranges the probability of error should increase rather than decrease. Although this may be true in general, it is possible in some limited cases for the converse to be true. To demonstrate this phenomenon, this portion of the experiment could be repeated for a larger target set with more ranges. Instead of continuing with this approach to the problem, however, work on a more general approach which related more directly to the performance of future algorithms was begun.

Section 4 General Correlation Approach

Some of the problems relating to the use of a specific, "first generation" target recognition algorithm for investigation of the performance of future algorithms have already been discussed. Other technical difficulties were encountered in carrying out the test. For example, in trying to determine the influence of sampling rate on algorithm performance, we had problems using imagery small enough for the algorithm to accept. For high sampling rates at medium ranges, the size of the target expressed in pixels was too large to fit in the ADASIM window, within which the target is segmented and features are measured.

There were other obstacles to using ADASIM. In order to get results which were truly representative of the optimal performance for each sampling rate, the algorithm would have to be trained on a large data set of imagery with that sampling rate. Every change to the FLIR system design would require that the algorithm be retrained, something which would require an enormous amount of imagery and time. It was factors such as these which led to the change in approach to the problem.

The new approach chosen, depicted in Figure 11, was composed of two basic operations, 1) the simulation of imagery from FLIRs with different designs and 2) an interframe measurement comparing the final simulated imagery with the starting imagery. The interframe measure chosen was linear correlation which is similar to the matching operation performed by some template matching algorithms in their classification phase. This approach assumes that an area of interest operation has already been performed and has indicated the presence of a possible target.

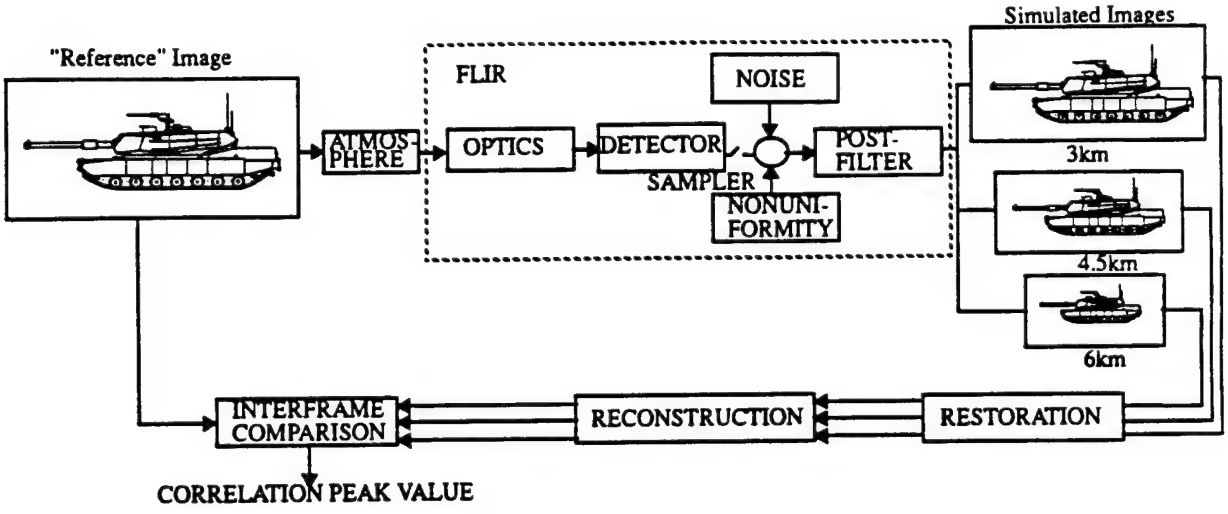

Figure 11. General correlation approach

Imagery of a target was first passed through a simulated atmosphere after which it was piped through the FLIR image chain. Elements of the FLIR image chain, the optics, detector, noise, nonuniformity, and postfilter along with restoration were the variables in this experiment. A

linear correlation was performed between the starting, high resolution image and the filtered image which had been reconstructed to the same size as the starting image using piecewise cubic reconstruction. A correlation surface was formed and the peak of the surface was used as a measure of the quality of the degraded image. It was also taken to be indicative of the quality of the imager. Since the quality was measured using a procedure which is similar to template matching, it is believed that comparison of the correlation peak values due to several simulated imagers is representative of the relative performance of future ATR algorithms, especially those which rely on template matching.

In fact, an argument can be made that the measured correlation values reflect an upper bound on performance of this type of algorithm. The template or model which is being matched, in this case the high resolution starting image, is as good a model of the target as one can possibly get. The target aspect is exactly that of the template. The choice of target-to-template orientation is also perfect, as is the choice of vehicle state (hot versus cold engine, hot versus cold treads, etc.). Any other choice of the target template (reference image) would result in a lower correlation value. Because correlation is thought to be related to relative performance of future algorithms, it is used as the basis of comparison for future FLIR designs.

The correlation measure has some disadvantages. It is a global measure, and, as such, it may not directly reflect the performance of algorithms which rely upon specific features of a target appearing in an image, for instance, an algorithm which looks for a gun barrel before it declares a target to be a tank. For algorithms such as these, a local measure of image quality might be more appropriate.

Correlation is also difficult to relate directly to range or some other typical figure of merit which can be used to quantify performance. The failure of our efforts to use a type of cross correlation to relate results to range will be discussed. The calculation of the correlation surface is computer intensive, and since a study like this should be done on a large ensemble of images in order to get good statistics, the computer time required to perform the test is enormous.

Despite the drawbacks of the correlation measure, it was thought to be the most representative of future algorithm performance and was used throughout the remainder of the study. Similar approaches have been taken by contractors in comparable efforts[5,6] however, this investigation is by far the most exhaustive.

4.1 THE IMAGING CHAIN

4.1.1 Targets

Imagery of the targets used as a reference set in this experiment is reproduced in Figure 12 through Figure 15 along with a histogram. The imagery was taken by a radiometer[7] at ranges less than 100 meters. The images were 480 x 512 pixels x 8 bits. We chose images with several pixels across the target for the reference image set so that we could consider the sampling in the reference image to be negligible when compared with the much coarser sampling to be simulated later in the image chain.

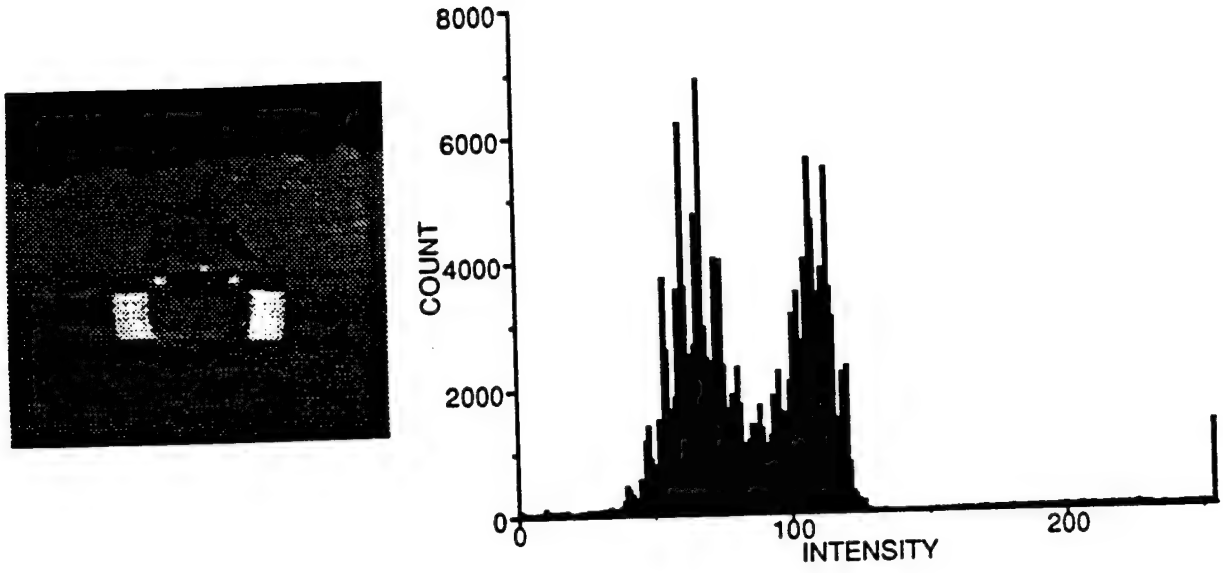

Figure 12. M60 front and the corresponding histogram

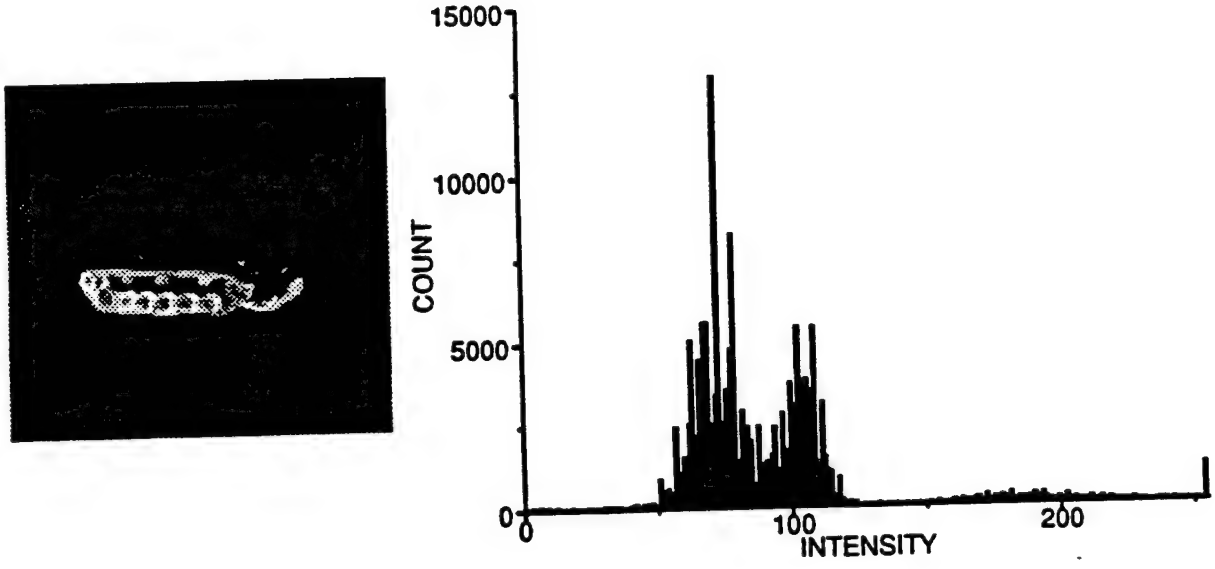

Figure 13. M60 right front and the corresponding histogram

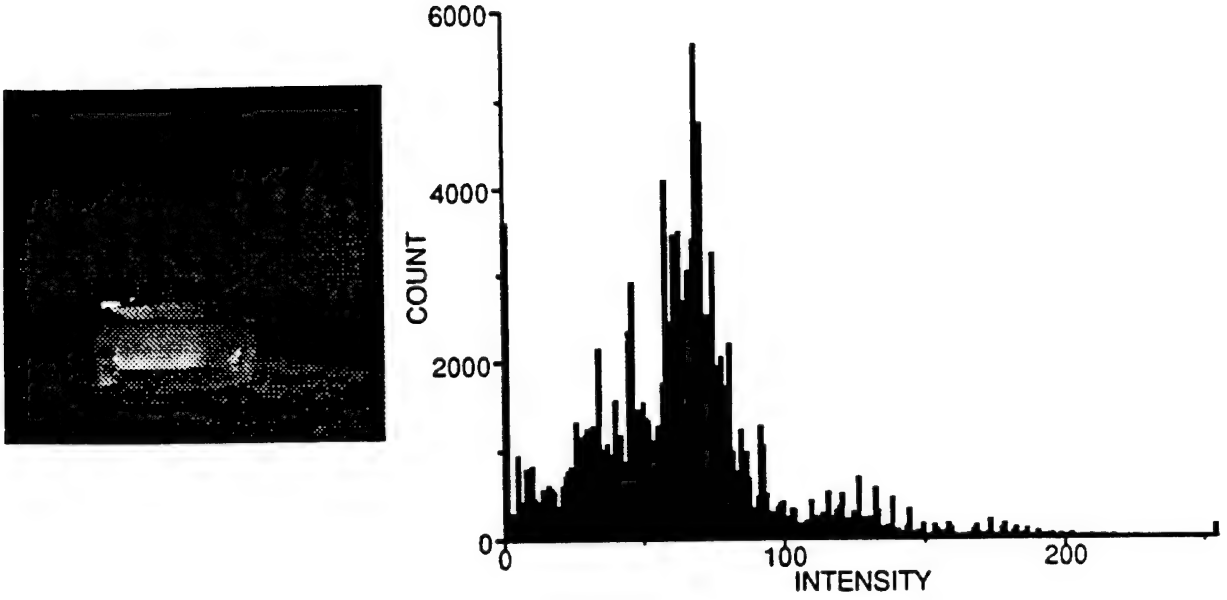

Figure 14. BMP front and the corresponding histogram

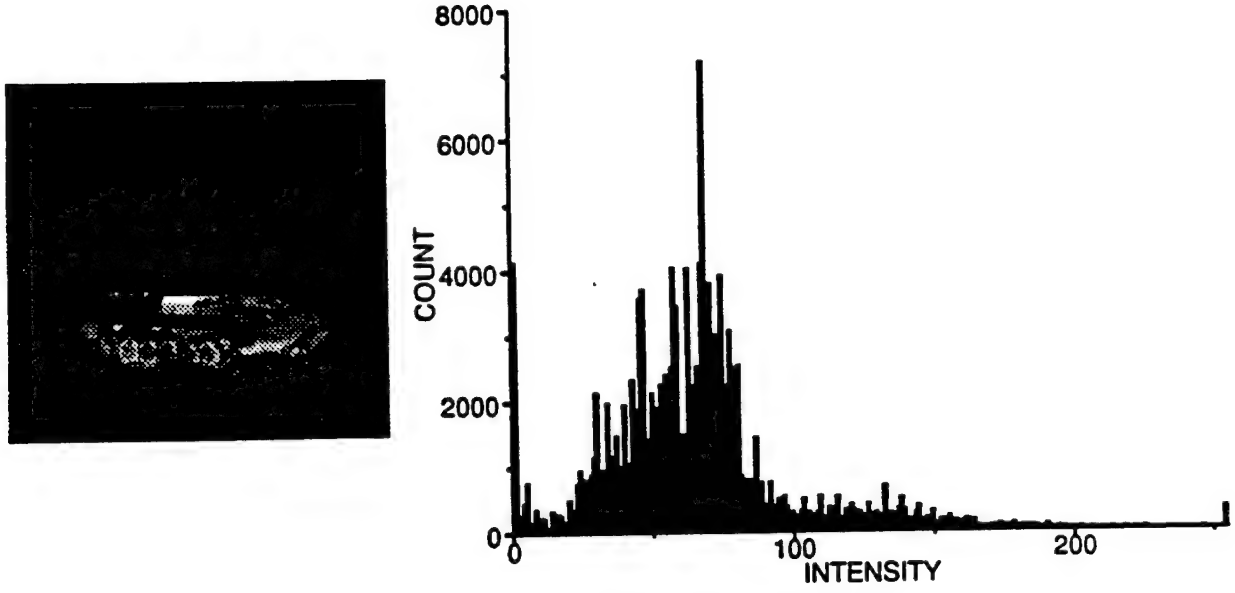

Figure 15. BMP right front and the corresponding histogram

4.1.2 Atmosphere

A simple Beer's law atmosphere was used to simulate the degraded contrast which would result from a typical atmosphere. The reduced contrast when combined later in the FLIR imaging chain with a signal independent noise results in a decreased signal to noise. The form for the attenuation used was

$$\Delta T_{Apparent} = |T_{Apparent} - T_{Ambient}| = |T_{Inherent} - T_{Ambient}| e^{-\sigma R} \qquad \text{(EQ 1)}$$

where $T_{Ambient}$ is the ambient temperature which was chosen to be equal to the mean of the image, $T_{Apparent}$ is the temperature of a scenel in the reference image after passing through the atmosphere, $T_{Inherent}$ is the scenel temperature before passing through the atmosphere, R is the range in km, and sigma is the attenuation coefficient in km^{-1}. (The term scenel will be used throughout this report to denote a picture element in the reference image. A separate term is used to distinguish it from a picture element in an image after application of the FLIR simulation which will be referred to as a pixel.) Two values of sigma were used, the first being 0.3 which corresponds to a relatively good atmosphere with approximately 74% transmission per km and the second value equal to 0.6 or approximately 54% per km. The ambient temperature in all cases was chosen to be the mean temperature of the image. The action of the atmosphere was to contract the histogram of the scene about the mean value of the target. Examples of imagery at 3 and 6 km with no atmosphere, the "good" and the "bad" atmosphere, along with their respective histograms are shown in Figure 16 through Figure 19.

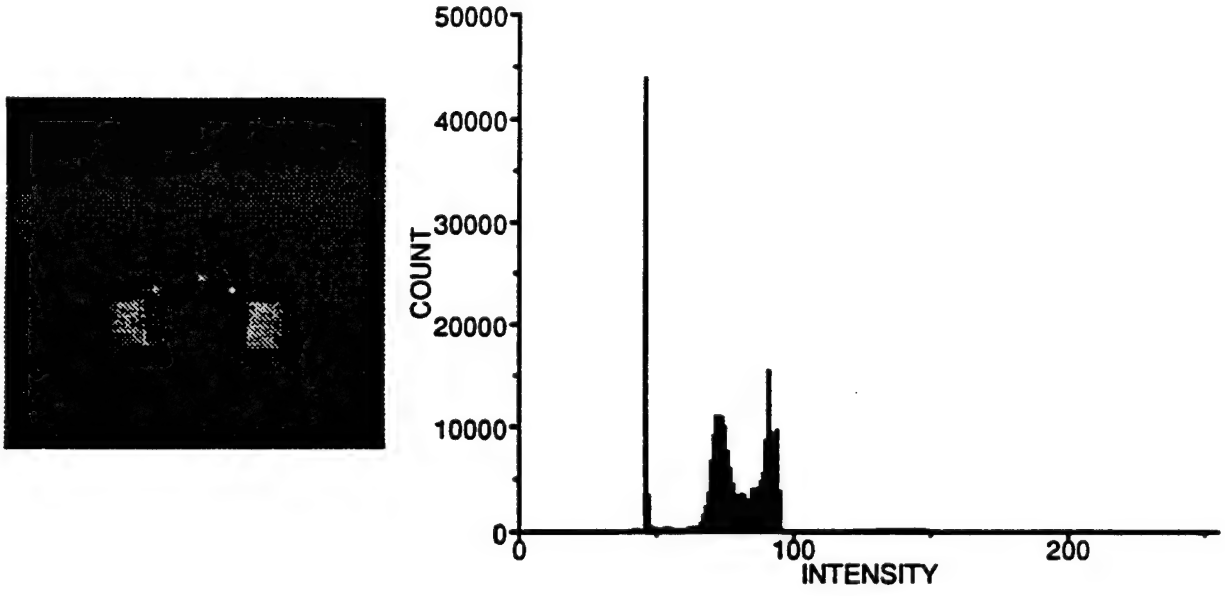

Figure 16. Example of imagery at 3km with "good" atmosphere

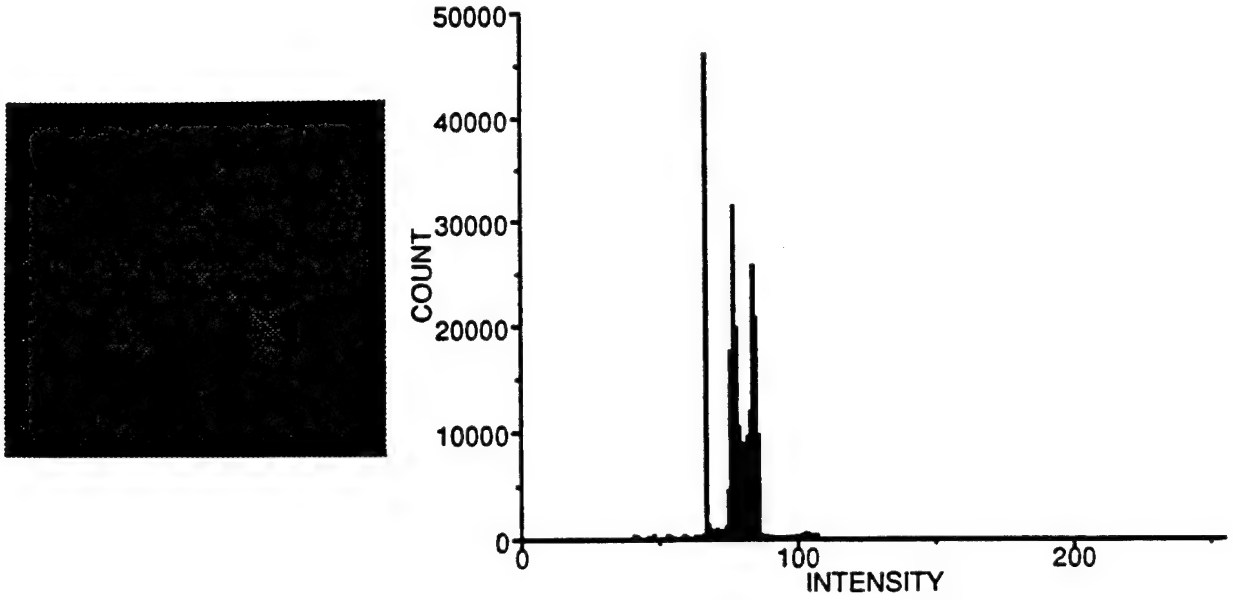

Figure 17. Example of imagery at 6km with "good" atmosphere

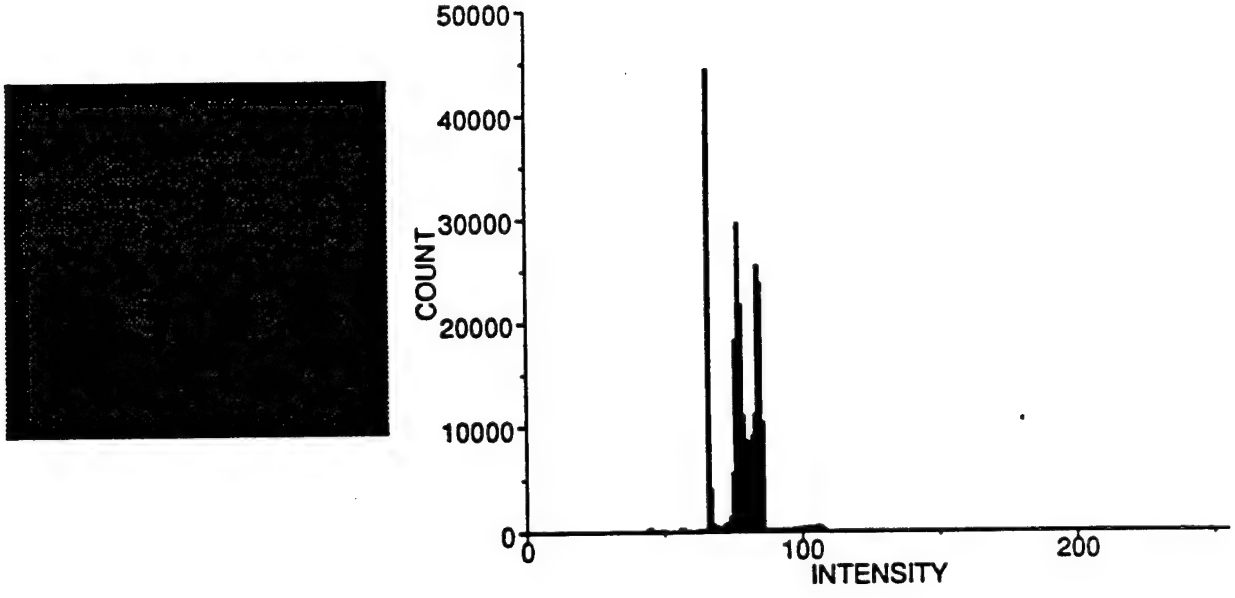

Figure 18. Example of imagery at 3km with "bad" atmosphere

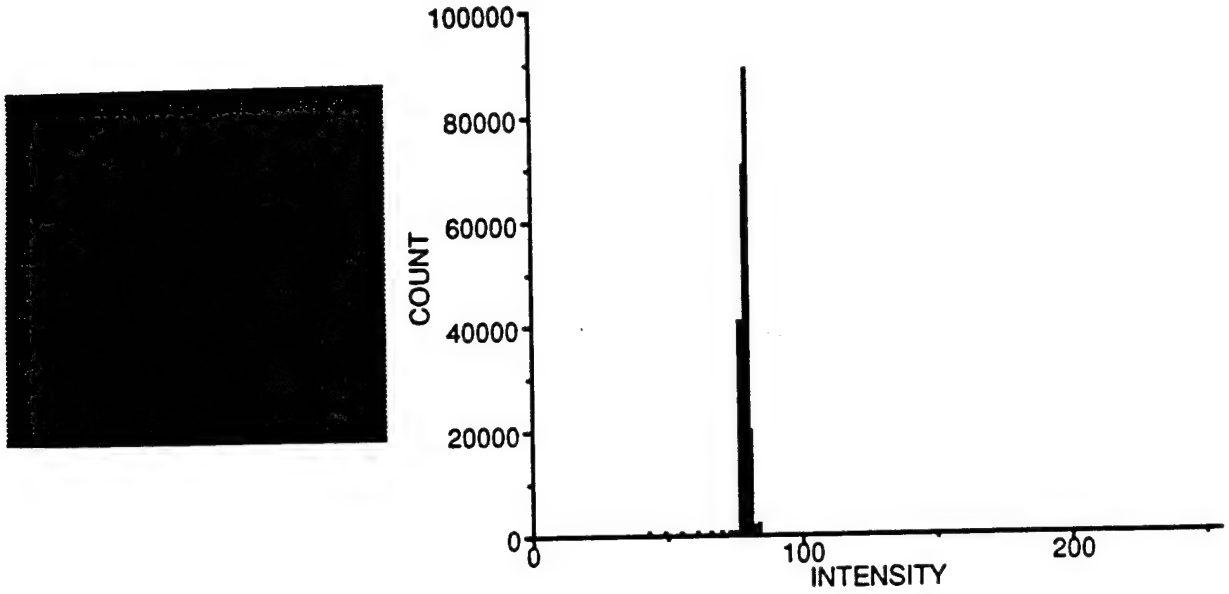

Figure 19. Example of imagery at 6km with "bad" atmosphere

4.1.3 FLIR

The components of the FLIR image processing chain and the simulation of each are covered in the following sections.

4.1.4 Optics

The optics of the simulated FLIR were assumed to be diffraction limited. Image formation on the FPA was simulated by convolving the atmospherically attenuated image with the diffraction pattern from a circular aperture which has the form:[8,9]

$$h_{opt}(r) = 2\left(\frac{J1(\pi(r/r_0))}{\pi(r/r_0)}\right)^2, \qquad \text{(EQ 2)}$$

where J1(r) is the Bessel function of order 1,

$$r = \sqrt{x^2 + y^2} \qquad \text{(EQ 3)}$$

and

$$r_0 = 1.22\lambda R/D \qquad \text{(EQ 4)}$$

where x and y are coordinates,
λ = wavelength of the IR radiation (10 µm), and
D= diameter of optics (0.203m).

By substituting the focal length for R above, the radius of the Airy disk at the focal plane was found to be 27.5 μm. To project the radius of the Airy disk into object space, (with respect to the reference image) one substitutes the simulated range to target for R (3, 4.5, or 6 km), resulting in 18, 27 and 36 cm respectively. In order to make the simulation more tractable, $h_{opt}(r)$ was truncated at $r=r_0$.

4.1.5 Detector, temporal integration and sampling

The image gathering operation of a detector which scans across an image plane can be separated mathematically into a term which characterizes the spatial response of the detector, a term which describes the temporal integration of the detector while scanning, and a term which defines the sample spacing. The detector spatial response here is assumed to be a rect function. The function which indicates the temporal extent of a sample is also a rect function. Sample spacing is described using a brush function, a regular 2-D array of Dirac delta functions.

The two rect functions are first convolved to produce a trapezoid or triangle function. This trapezoid, after being appropriately sized with respect to the reference image, could then be convolved with the whole image in order to account for the blurring due to the detector. The brush function could then operate on the image so that samples are chosen at the appropriate intervals. Instead of actually performing all operations separately, it requires far less computation to combine the convolution and sampling into one operation by simply placing the trapezoid functions at the appropriate sample spacings and summing the weighted contributions from the trapezoid.

There are three separate grids which come into play in this sampling. First, there is the grid defining the reference image scenels, which have a particular angular separation at a given range. The second grid is one which describes the detector spatial response combined with integration while scanning. Each element of the detector array is projected out to the simulated range and overlaid onto the grid of the reference image. Bilinear interpolation is performed to compute the input image's response to each detector template element. These values are summed over the entire detector to form one sample. The third grid corresponds to the sampled image.

Normally the sampling operation is begun by placing the detector template exactly in the upper left hand corner of the reference image. The influence of sample-scene phasing can be investigated by simply starting the sampling operation shifted by a fraction of a detector template with respect to the reference image. This was done at nine evenly spaced positions within the unit cell formed by four adjacent samples (See Figure 20).

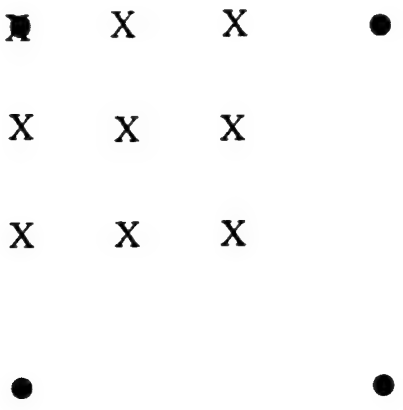

Figure 20. Unit cell of the sampling grid (dots) and different positions (Xs) chosen to simulate the effects of sample-scene phasing.

4.1.6 Interlace

The influence of interlace misregistration was previously investigated (see Section 3 on page 5) using terrain board imagery which had every other line of imagery shifted either vertically or horizontally. The shifted images were then operated on by the ADASIM algorithm. The approach could be questioned since interpolation was required to form one field and not the other. This would filter the interpolated field and not the other field, perhaps influencing the results.

A different approach using the FLIR simulation was used in this portion of the experiment. In a manner similar to that used to produce imagery with different sample scene phases, imagery with specific amounts of interlace misregistration, both vertically and horizontally, were produced. The operation did not filter one part of the image more than another and thus was thought to be more realistic.

4.1.7 Noise

In real imaging systems some detectors are noisier than others. For parallel scanned imagers this produces a row to row variation in the amount of noise in the final image. For this experiment we have specified noise distributions for each row of the image. For the first three noise cases the noise along a particular row was chosen randomly from a Gaussian distribution with a mean of zero. The standard deviation of the distribution for each row, σ_r, was also randomly chosen from a Gaussian distribution with nonzero mean μ and standard deviation σ. Parameters summarizing the three noise levels investigated are presented in Table 3. For the fourth noise case σ_r was chosen to be a constant for the whole image, the value of the constant varied with detector area.

Table 3. Parameters of the Gaussian distribution of σ_r corresponding to noise added expressed in quantization levels

Noise Level	m	s
1	1	2
2	2	2
3	4	4

The mean values of the distributions were chosen to span typical FLIR design philosophies. That is, some FLIR designers indicate that they design a FLIR so that the magnitude of the least significant quantization level is equal to the system Noise Equivalent Temperature difference (NET).[10] Other designers advocate quantizing the dynamic range so that there are four quantization levels within the temperature span of one NET. Their arguments for one choice or another center around the required thermal dynamic range as well as the visibility of noise after the human visual system has spatially and temporally integrated the scene.

Imagery which is representative of the three noise levels is shown in Figure 21.

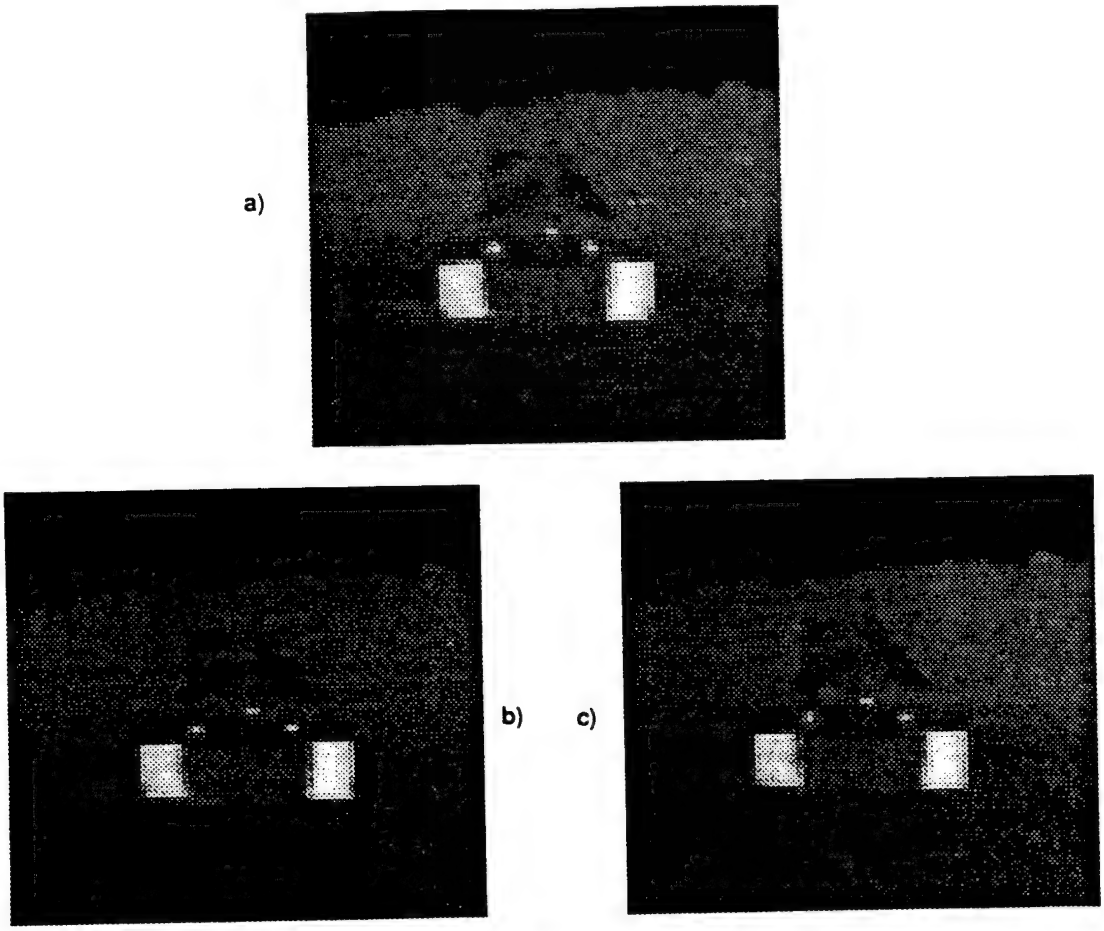

Figure 21. Representative imagery with noise a) level 1, b) level 2, c) level 3

Another experiment was performed where it was assumed that the system was a BLIP (Background LImited Photodetector) system.

For tactical infrared imagers the ultimate sensitivity of the imaging system is achieved when the dominant noise source results from the fluctuation in the number of photons arriving from the scene.[11] For a system which is limited by this type of noise, called a BLIP limited (Background LImited Photodetector) system, a larger detector is advantageous from a SNR standpoint. The probability of arrival of a photon at a detector can be approximately described by a Poisson distribution. The SNR measured after the detector is the square root of the mean number of photons arriving during a particular time interval. A larger mean number of photons will be incident upon a detector with larger angular subtense (or larger physical area if the optics is kept constant), resulting in a higher SNR in the final image.

For a BLIP system the signal is taken to be equal to the mean number of photons, which in turn is proportional to the detector area. The variance of the Poisson process is the mean, and the RMS noise level is the square root of the mean number of photons. The signal to RMS noise level is then proportional to the square root of the mean, and thus proportional to the square root of the detector area. In this experiment the variation of SNR with changing detector area was accomplished by varying the amount of noise added to the image.

This improvement in SNR for larger detectors will act to improve the final correlation between the simulated and reference images. At the same time the decreased resolution due to the larger detectors will degrade the correlation indicating that optimal system design ultimately involves a trade-off between system sensitivity and resolution. This improvement in system SNR due to choice of a larger detector could be used to increase the system dynamic range, or could be used to decrease the size of a quantization level (as expressed in degrees K). Both modifications to the system design would require increased system bandwidth however.

For the cases where noise was treated independently of detector area and for the BLIP detectors where the noise was tied to the detector area the mean values of the distributions describing the variances were chosen to span typical FLIR design philosophies. That is, some contractors have indicated that they have designed a FLIR so that the magnitude of the least significant quantization level is equal to the system NET. Others advocate quantizing so that there are four quantization levels within the temperature span of one NET. Their arguments for one choice or another center around the visibility of noise after the human has spatially and temporally integrated the scene.

4.1.8 Nonuniformity

The nonuniformity being simulated in this portion of the simulation is residual nonuniformity in the image after correction. In general, the form of the residual spatial noise in an image after implementation of a linear n-point correction scheme is a complicated function of the number of correction points and the temperature spread between the points.[12] Simulation of the exact form of the spatial noise vs. input photon flux for our application would have been an unnecessary complication. Instead we chose a much simpler approximate way to simulate the residual nonuniformity.

The nonuniformity of each simulated detector's response to signal is assumed to be of unity gain in all cases. The offset for each simulated line is assumed to be constant for the whole line. The value of the offset is the result of a random draw from a Gaussian distribution of possible offsets described by a mean of zero and a standard deviation of 1, 4 or 8 quantization levels, corresponding to nonuniformity levels 1, 2 and 3 respectively. Table 4 gives the statistics for the offset distribution for the 3 nonuniformity levels.

Table 4. Nonuniformity levels simulated and the corresponding mean and standard deviation values quoted in units of quantization levels or bits for gain and offset distributions

Level	mean of gain	std. dev. of gain	mean of offset	std. dev. of offset
1	0	0	0	1
2	0	0	0	4
3	0	0	0	8

The variance in signal for a flat field in the cross scan direction is seen to be the same order of magnitude as the variance of the noise. They are both chosen to be of the same order of magnitude as a system NET to which systems are designed. Of course actual system performance of second generation prototypes has not always achieved the level of performance specified for the system. Examples of imagery with nonuniformity levels 1, 2, and 3 are shown in Figure 22.

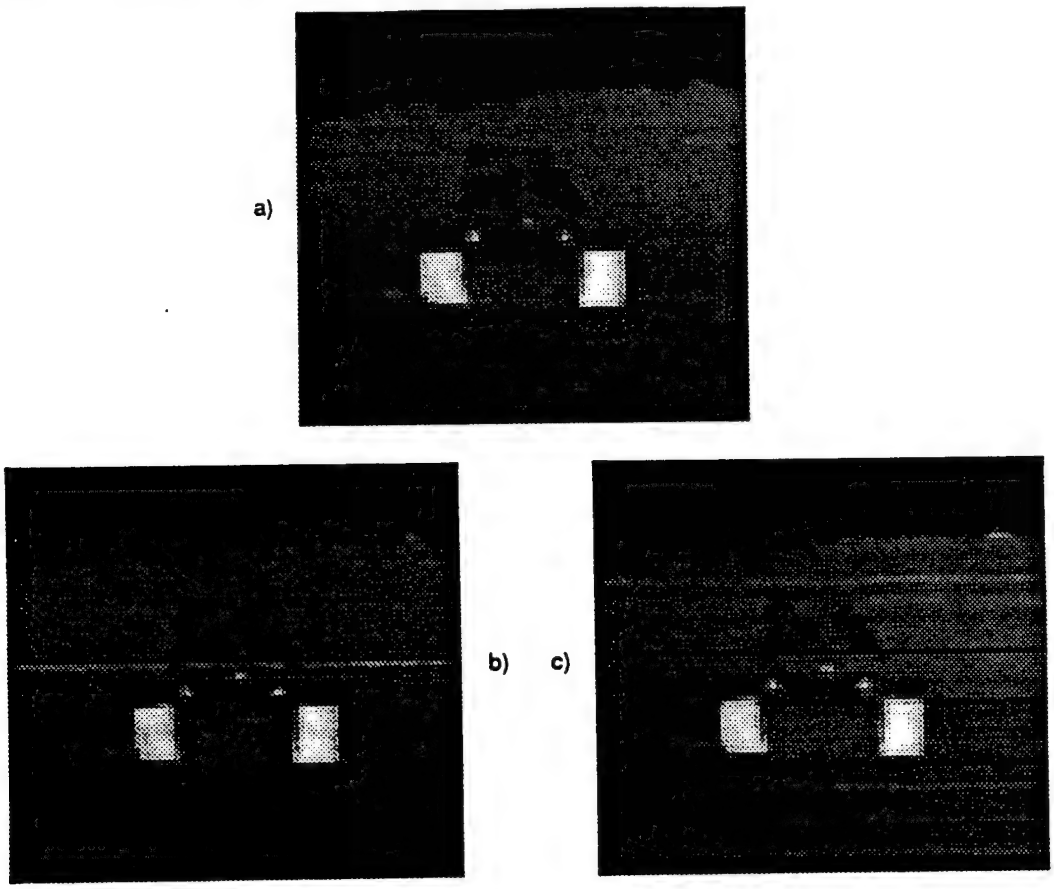

Figure 22. Examples of imagery with simulated nonuniformity a) level 1, b) level 2, c) level 3

4.1.9 Reconstruction

Once the image has been processed by the FLIR simulation, the resultant image is much smaller than the reference image due to sampling. In order to compare the result with the original, the output image must be rescaled to the original image size. For an example see Figure 23. The sampled images were reconstructed to their original pixel size using a two parameter piecewise-cubic convolution algorithm. The scale factor used was the ratio of input image size to output image size.

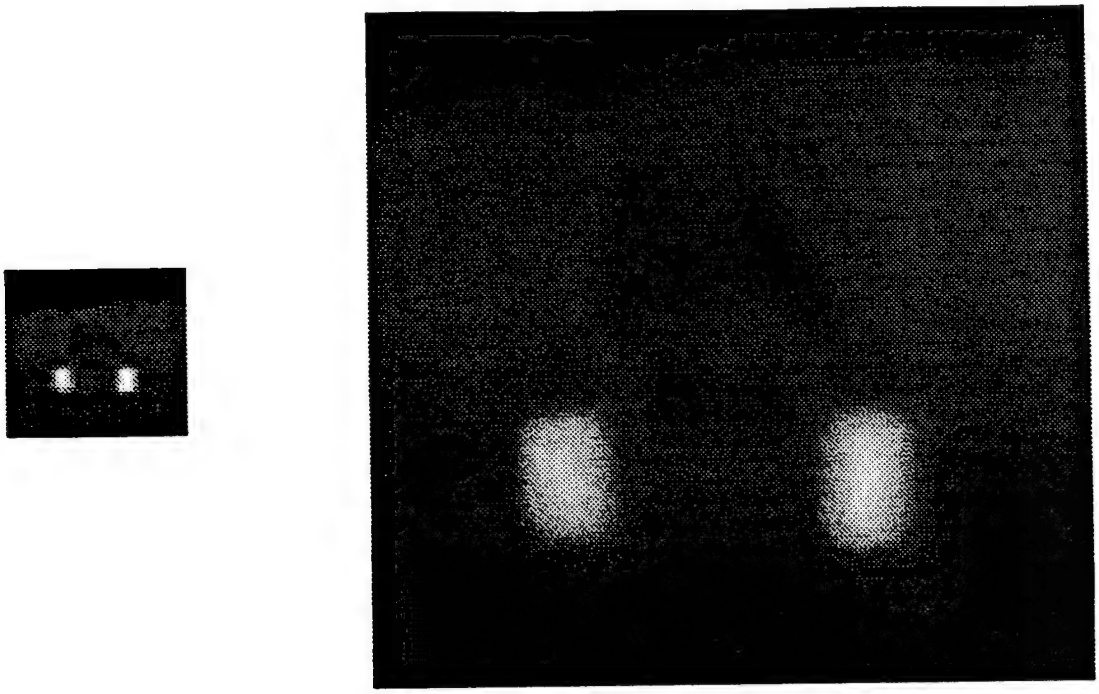

Figure 23. Examples of sampled and then reconstructed imagery (not to scale)

One-dimensional piecewise-cubic reconstruction is implemented by convolving the samples of a sampled image g with a piecewise-cubic kernel r to define the continuous result G

$$G(x) = \sum_{n=-\infty}^{\infty} g[n]\, r(x-n) \qquad , -\infty < x < \infty$$

The two parameter cubic function r is given by

$$r(x) = \begin{cases} (2+\alpha-6\beta)\,|x|^3 + (-3-\alpha+9\beta)\,|x|^2 + (1-2\beta), & |x| < 1 \\ (\alpha+2\beta)\,|x|^3 - (5\alpha+9\beta)\,|x|^2 + (8\alpha+12\beta)\,|x| - (4\alpha+4\beta), & 1 < |x| \le 2 \\ 0, \textit{ otherwise} \end{cases}$$

This reconstruction method was shown by Park and Reichenbach[13] to minimize mean square error at low frequencies when α=-0.5, β=0.0. The algorithm uses a small kernel size to efficiently fit sampled data to a piecewise cubic function.

For α = - 0.5, and β = 0.0, r(x) interpolates the sampled image and minimizes mean square error between reconstructed image and the original image. When α = -0.5, and β = 1/6, r(x) approximates the cubic B-spline. Since the image data used in the experiments contained sharp edges, and thus high frequency information, reconstruction with α = -0.5, β = 0.0 led to some reconstructed pixels having negative values, so the parameter settings of α = -0.5, and β = 1/6 were used in the experiments.

Since r(x) is non-zero only for $|x| \leq 2$, only four points are needed from the sampled image to reconstruct each intermediate pixel. If the scale factor for reconstruction is S, then to fill in the jth point between adjacent input pixels X and X+1 from sampled image g:

$$h(SX + j) = \sum_{k=-1}^{2} g(X + k)\, r\left(\frac{j}{S} - k\right), 0 \leq j \leq (\lfloor SX + 1 \rfloor - \lfloor SX \rfloor - 1)$$

The reason j ranges as above is that the scale factor S is not necessarily an integer.

The reconstruction was done in two parts. First, the image was rescaled horizontally; then that array was scaled vertically to achieve the original image size.

4.2 INTERFRAME COMPARISON - CORRELATION

After FPA parameter changes were made to a FLIR image and the image was rescaled to its approximate original size, a method was needed to compare the rescaled image to its reference image. Linear correlation provided a consistent measure for comparison of the rescaled and reference images. The main reason correlation was chosen was the similarity of correlation with the operation of template matching. It also gave numerical values which could be used to determine which FPA parameter changes affected FLIR performance. Correlation values could be used to rank the relative effects of the various FPA parameter changes: samples/IFOV, sample scene phasing, atmosphere, detector size and shape, noise, and nonuniformity.

The linear correlation coefficient r is given by the formula:

$$r = \frac{\sum_i (x_i - \bar{x})(y_i - \bar{y})}{\sqrt{\sum_i (x_i - \bar{x})^2}\ \sqrt{\sum_i (y_i - \bar{y})^2}}$$

where $\bar{x}$ is the sample mean of the x 's (pixel values of the reference image), and y is the sample mean of the $\bar{y}$'s (pixel values of the rescaled image). The value of r lies between -1 and 1, inclusive. It takes on a value of 1, termed "complete positive corhen two images are exact replicas of each other. A value of r near 0 indicates that the two images are uncorrelated. When r has the value -1, the two images have "complete negative correlation."

The correlation method is extremely calculation intensive. Because the rescaled image was smaller than the reference image, it was necessary to shift the rescaled image over the reference image and calculate individual correlations for each alignment of the two images. This procedure involved matching the centroids of the two images, shifting the rescaled image one pixel's distance in a 24x24 pixel grid around the centroid of the reference image, and using the given correlation formula to calculate a correlation value at each new location of the rescaled image. Although this process involved making 576 separate correlations between the two images, each of which contained from 200,000 to 250,000 pixels, it insured that the peak correlation value was determined by the best alignment of the two images. To minimize round off error, all calculations were performed with floating point pixel values rounded to six decimal places. This increased the correlation calculation time, but gave a more precise correlation value, especially in view of the fact that up to 500,000 pixel values were involved in calculating one correlation between the two images.

4.3 TEST SOFTWARE

Subroutines were created to simulate each of the different operations of the atmosphere and FLIR. An input image was operated on by each in turn. Finally, correlation was calculated between the resulting and starting images. The whole procedure was controlled through the use of a piping system and experiment files, the details of which are presented in Section A-1. The piping system worked extremely well because it allowed many variations of FPA parameter changes to be made while the experiment was in progress.

Section 5 Results Using Correlation Approach

The different combinations of variables tested and their values are presented in Table 5. Each column describes those variable values used in a particular experiment. The results of each of the eight experiments will be discussed in the next eight sections. In all cases the values of the variables used in the test were chosen to span those values typical of first generation systems and proposed second generation FLIRs. Specifically, we addressed issues pertinent to the IRFPA program. Addition of more detectors, higher sampling rates, more stringent noise and nonuniformity specifications, and going to a noninterlaced design all tended to drive up the cost of proposed second generation focal plane arrays.

Table 5. Test variable matrix

	Noise	Atmos-phere	Atmos-phere& Noise	Nonuni-formity	Atmos-phere& Nonuni	Sampling Square Detector	Sampling Detector Asp.Ratio	Sample Scene Phase
TARGETS								
M60Front	X	X	X	X	X	X	X	X
M60RtFront						X		
BMPFront						X		
BMPRtFront						X		
RANGE								
3000m	X	X	X	X	X	X	X	X
4500m	X		X	X	X	X	X	X
6000m	X	X	X	X	X	X	X	X
ATMOSPHERE								
sigma 0.0 none	X	X		X		X	X	X
0.1		X						
0.2		X						
0.3 good		X	X		X			
0.4		X						
0.5		X						
0.6 bad		X	X		X			
OPTICS	X	X	X	X	X	X	X	X
DETECTOR SIZE								
IFOV-x width (mrads)								
0.05							X	X
0.08	X	X	X	X	X	X	X	X
0.12						X	X	
IFOV-y height (mrads)								
0.05						X	X	
0.08	X	X	X	X	X	X	X	X
0.12						X	X	
0.16							X	
SAMPLES/IFOV-x&y								
1.0						X	X	X
1.5	X	X	X	X	X	X	X	X
2.0						X	X	X

Table 5. Test variable matrix (continued)

	Noise	Atmos-phere	Atmos-phere& Noise	Nonuni-formity	Atmos-phere& Nonuni	Sampling Square Detector	Sampling Detector Asp.Ratio	Sample Scene Phase
SAMPLE SCENE PHASE								
none-1 frame	X	X	X	X	X	X	X	X
3x3- 9 frames								X
NOISE 4FR.								
level 1	X		X					
level 2	X		X					
level 3	X		X					
level 4			X					
NONUNIFORMITY 6FR.								
level 1				X	X			
level 2				X	X			
level 3				X	X			
CROSSCORRELATION								
M60Fr - M60Fr	X	X	X	X	X	X	X	X
M60Fr - M60RtFr			X					X
M60Fr - BMPFr			X					X
M60Fr - BMPRtFr			X					X

Noise Level	μ	σ
1	1	2
2	2	2
3	4	4

Level	mean of gain	std. dev. of gain	mean of offset	std. dev. of offset offset
1	0	0	0	1
2	0	0	0	4
3	0	0	0	8

In the first few tests, variables were tested one at a time, not only to determine the influence a particular variable had on ATR performance but also to determine the range of parameter values which began to have an appreciable influence on correlation. In this way the first few tests provided information which allowed us to decide whether certain tests should be performed, and if they should, what was the best choice of starting parameters for those tests involving combinations of variables. For those combinations of variables which one would expect to be strongly coupled, for example sampling rate and detector IFOV, values of the two variables were varied systematically over a range which spanned possible first and second generation system designs.

For most of the testing the image of the M60 tank front was used as the reference image. The simulation was performed at ranges of 3, 4.5 and 6 km, thus, spanning tactically relevant ranges. The optics F/# was 2.25 for all cases. Atmosphere was not included unless specified.

Three variables explored were assumed to be random: noise, nonuniformity and sample-scene phase. That is, a series of images with the same level of noise, but with different starting seeds in the randomization routine which generated the noise, resulted in different values of correlation. For the chosen values of noise, we had to determine the spread in correlation values and how the spread changed with range. In the case of sample-scene phase, the parameter which is analogous to the starting seed of the random number generator for noise is the starting position of the sampling grid within a unit cell. For a real system the phasing effects would manifest themselves whenever the system LOS was changed.

One would expect that noise and nonuniformity might have a strong coupling with signal level (as determined by the signal level in the reference image and the atmospheric attenuation). Since the signal level decreases with range due to atmospheric attenuation, it is expected that any appreciable spread in correlation values due to noise or nonuniformity would increase with range. One would also expect that sample-scene phasing would be closely coupled with sampling rate and detector size. A few of these random variables were investigated in the first phases of the testing in order to determine the magnitude of their influence on correlation. If their magnitude were determined to be large, we then investigated the coupling between them and other variables.

5.1 NOISE

The system simulated in this portion of the test had a square IFOV with 1.5 samples per detector subtense in both directions. The optics F/# was 2.25. The same basic system design was used in several of the following experiments.

Four images of each of the three noise levels were created at each of the three ranges (see Figure 21). Figure 24 is a plot of the results which indicate very little degradation of the correlation due to noise alone. Also note that the spread of correlation values is almost negligible.

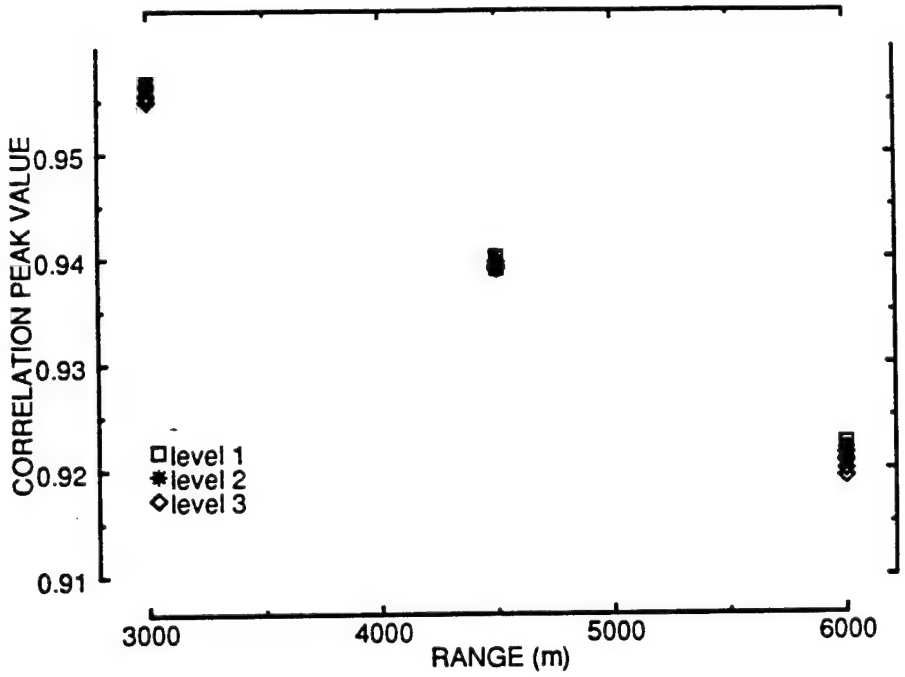

Figure 24. Plot of correlation vs. range for 3 noise levels

Level	mean of gain	std. dev. of gain	mean of offset	std. dev. of offset offset
1	0	0	1	2
2	0	0	2	2
3	0	0	4	4

If one compares this result with those for the same system with no noise, which is plotted as curve 2 in Figure 32, (see Section 5.7 on page 58) the degradation of correlation with range is seen to be almost totally due to optics, detector, and sampling, with hardly any contribution of the noise levels.

5.2 ATMOSPHERE

For the same basic system described in section 5.1 above without noise, we investigated the influence of atmosphere. Correlation values of the imagery degraded by no atmosphere and the good and bad atmosphere are plotted vs. range in Figure 25. One notices that there is negligible degradation of the correlation due to the atmosphere alone.

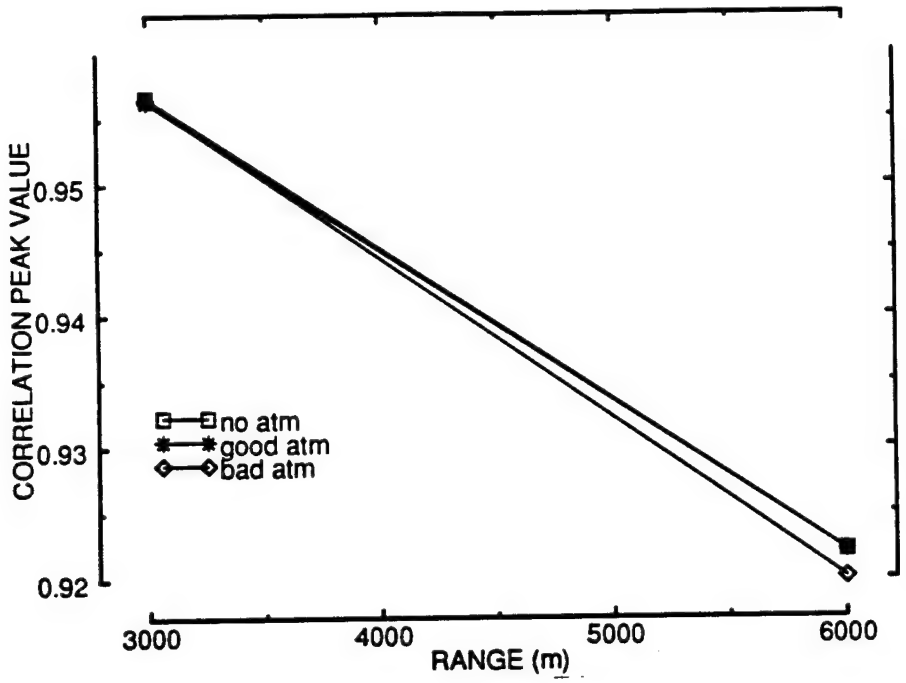

Figure 25. Correlation vs. range for no atmosphere, "good" atmosphere and "bad" atmospheres

We next tested the interaction of noise and the variable which strongly influenced signal level: atmosphere. It was felt that trying to look for a coupling of noise with other variables related to resolution would not be fruitful.

5.3 NOISE WITH ATMOSPHERE

For the same basic system and ranges as in section 5.1, we added both noise and atmospheric attenuation. The results plotted in Figure 26 indicate a dramatic degradation of correlation for the poor atmosphere. (n.b. The y axes will change from one presentation of experimental results to the next in the following figures.) As in the previous experiment dealing with noise, four images with the same noise level were created at each range. The spread of correlation values becomes significant at longer ranges especially for the poorer atmosphere where the signal to noise is low. The imagery becomes almost unrecognizable for low correlation values, 0 to approximately 0.5 or 0.6.

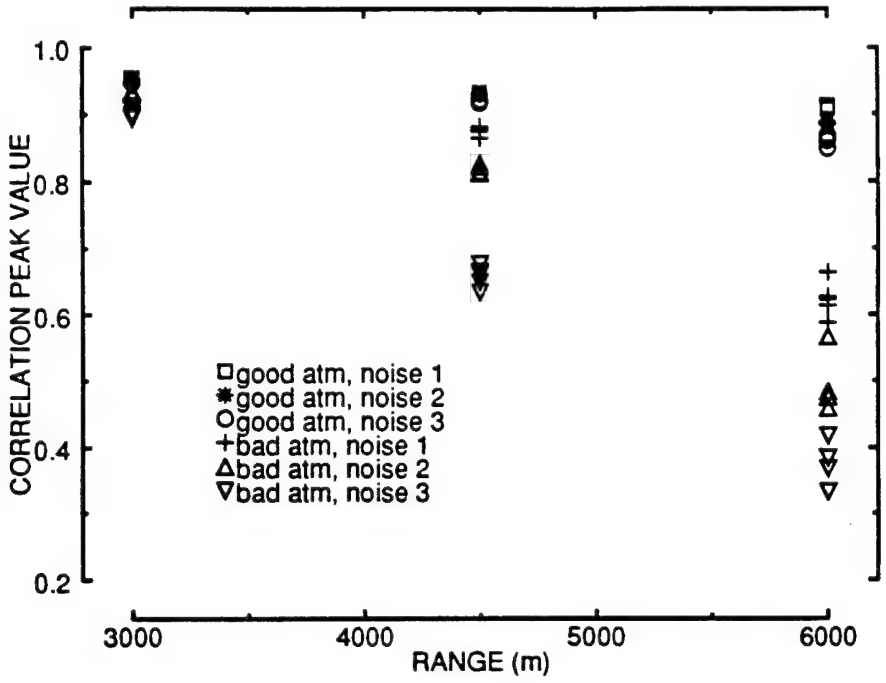

Figure 26. Correlation versus range for two different atmospheres and three different noise levels

5.4 NONUNIFORMITY

Again, for this experiment the basic FLIR system design was kept the same as in the previous tests. Three different levels of nonuniformity, as described in Section 4.1.8 on page 25, were added to the imagery. No atmosphere was simulated. Six frames of each nonuniformity level were created at each range. The results which are plotted in Figure 27 indicate little degradation in correlation value except for the highest level of nonuniformity, level 3. The spread in correlation is significant only for level 3 as well.

Present FLIR system designs are tending toward increased dynamic range, on the order of ten to twelve bits spread over a temperature range of 40 to 50 degrees. Uncorrected nonuniformity values can be very large for HgCdTe, on the order of 10% of the total dynamic range. After correction the goal of most system designs is to get the nonuniformity smaller than an NET. It

depends on the contractor design philosophy as to whether they try to set an NET equal to a least significant bit or whether they try to digitize the NET. The level of nonunifomity represented by level 3 is perhaps close to what one might expect for poorly corrected HgCdTe imagery.

For a human looking at a displayed image sequence, the streaking resulting from uncorrected nonuniformity is emphasized by the temporal integration of the eye. On the other hand, the temporal integration of the eye tends to minimize the impact of random temporal noise in an image sequence.

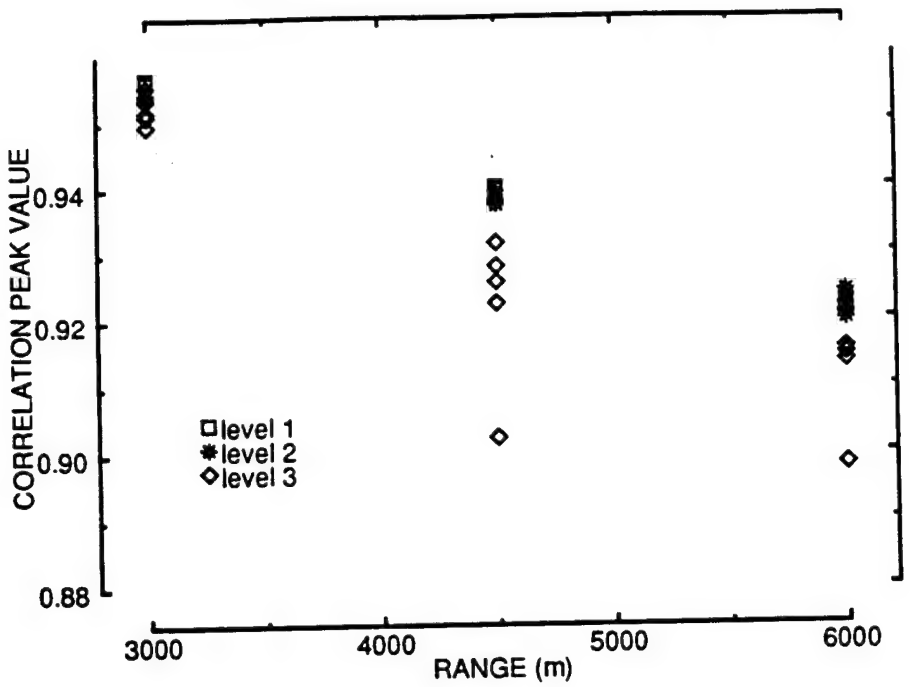

Figure 27. Correlation vs. range for different levels of nonuniformity alone

Nonuni Level	mean of offset mean	std. dev. of offset mean	mean of offset std. dev.	std. dev. of offset offset std. dev.
1	0	0	0	1
2	0	0	0	4
3	0	0	0	8

5.5 ATMOSPHERE AND NONUNIFORMITY

Keeping the basic FLIR design consistent with previous experiments, we looked at the influence of atmosphere with nonuniformity. Figure 28 is a plot of the results which are similar to those for the noise plus atmosphere case. For the "good" atmosphere there was little degradation of correlation with range; however, for the bad atmosphere the degradation with range is even more pronounced than for the worst noise case.

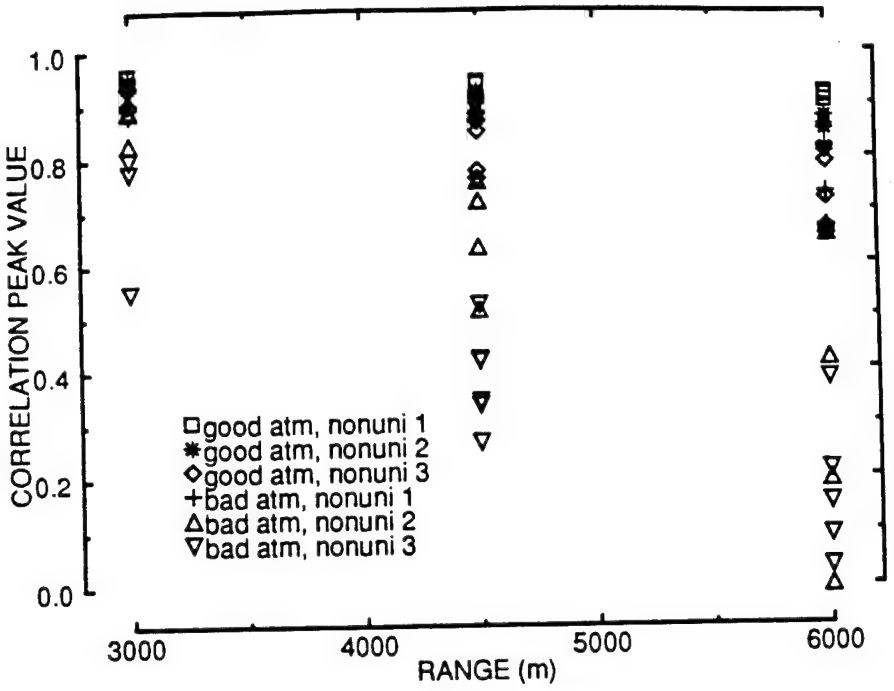

Figure 28. Atmosphere plus nonuniformity

5.6 INTERLACE MISREGISTRATION

Using the basic FLIR design as in the previous tests, we varied the misregistration of fields as discussed in paragraph 2 of Section 4.1.6 on page 23 and looked at the correlation peak value versus range. Figure 29 and Figure 30 show results of misregistration in the x and y directions respectively. Degradation in correlation is not very large between the case of no misregistration and the quarter or half pixel misregistration cases (between line 1 and lines 2 or 3 of the graph in Figure 29 and Figure 30) in either the x or y direction. However, for one and two pixel misregistration in both directions, the degradation is significant.

Second generation FLIR systems usually limit the LOS jitter to a small portion of an IFOV (typically less than 20%). If this is the case, the interaction of an interlaced scan with residual jitter would probably not produce large misregistrations on the order of 2 pixels. Improper timing could produce such an image defect.

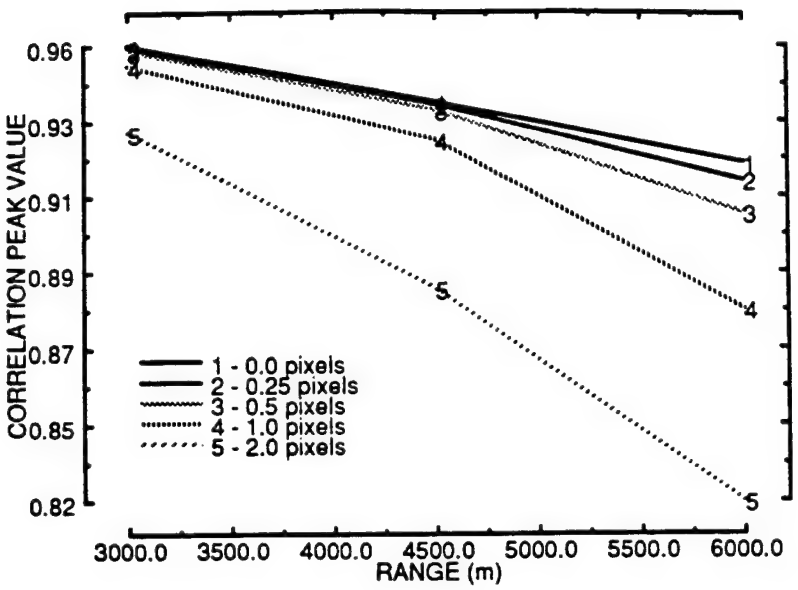

Figure 29. Correlation vs. Range for misregistration in X direction

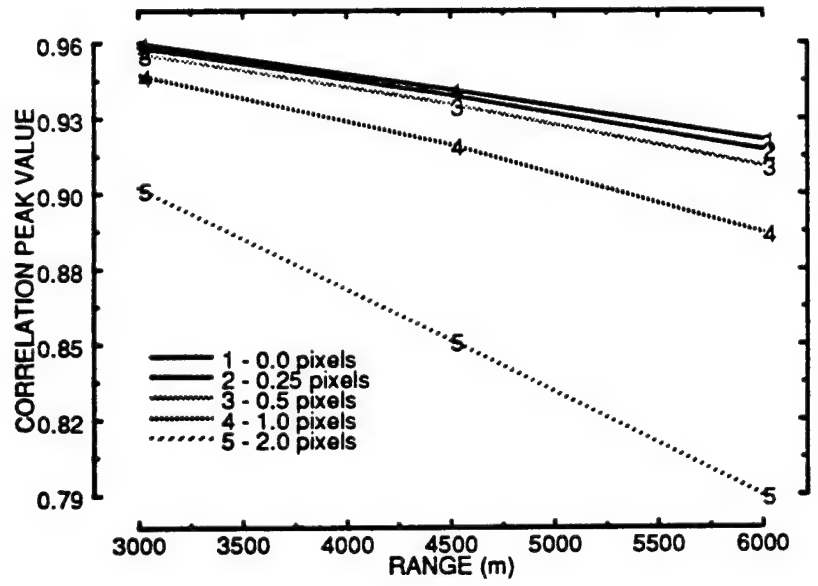

Figure 30. Correlation vs. Range for misregistration in Y direction

5.7 SAMPLING USING SQUARE DETECTORS

The basic FLIR system simulated was the same as in previous experiments except for the simultaneous variation of the sampling rate and detector size in both directions. Figure 31 shows the relative sizes of the square detectors and the sampling grid for the cases simulated in the experiment. Table 6 describes detector dimensions and sample spacings for both square and rectangular detectors. As can be seen from Figure 32, the improvement in correlation in going from 1 to 1.5 samples per dwell (spd) is larger than the improvement in going from 1.5 to 2 spd.

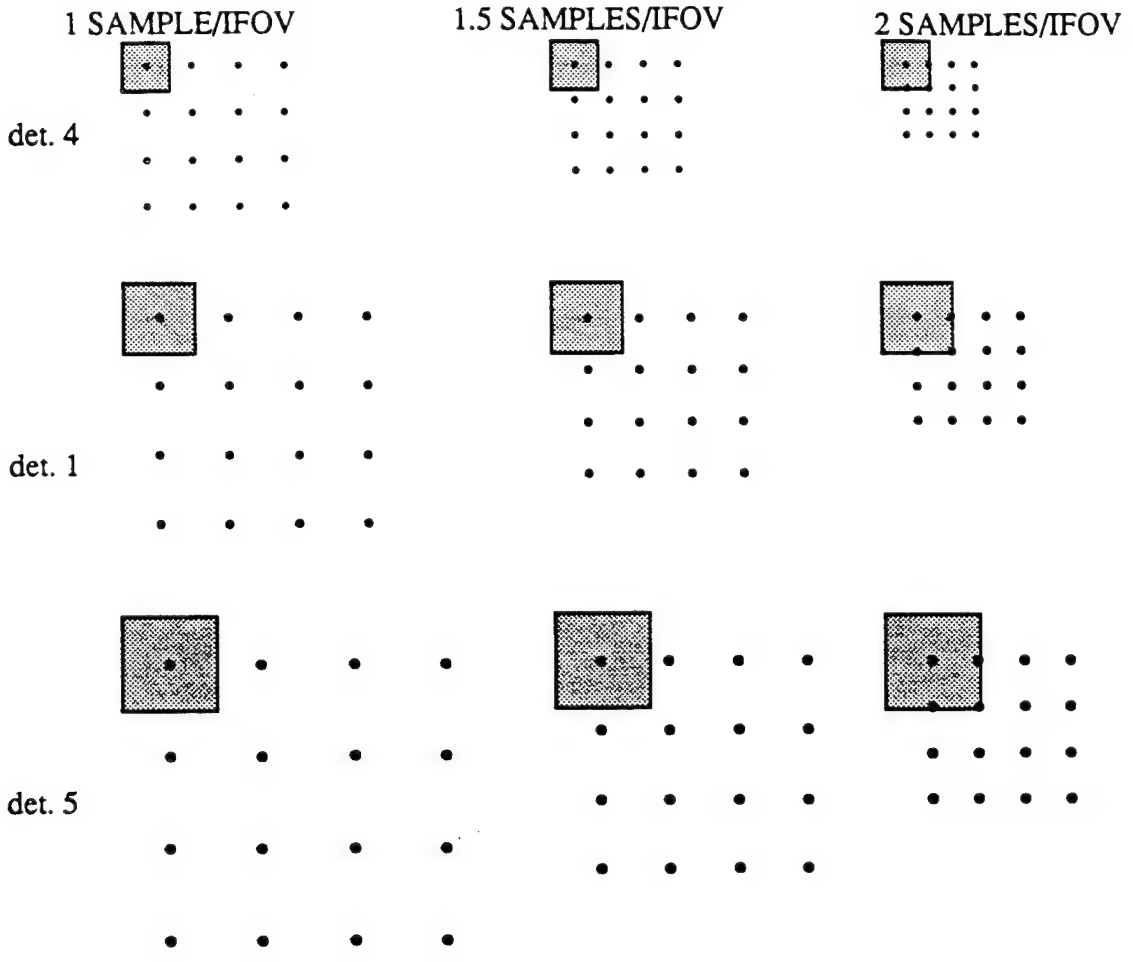

Figure 31. Relative size of square detectors (shaded squares) and square sampling grids(dots)

Table 6. Detector and sampling descriptions

DETECTOR NUMBER	DETECTOR SIZE X DIMENSION μM (μRads)	DETECTOR SIZE μM (μRads)	# SAMPLE PER IFOV (μRads)	SAMPLE SPACING X DIMENSION μM (μRads)	SAMPLE SPACING Y DIMENSION μM (μRads)	SAMPLE DENSITY (SAMPLES/MRAD^2)
1	36.6 (80)	36.6 (80)	1.0	36.6 (80)	36.6 (80)	156
			1.5	24.4 (54)	24.4 (54)	351
			2.0	18.3 (40)	18.3 (40)	625
2	36.6 (80)	54.84 (120)	1.0	36.6 (80)	54.84 (120)	104
			1.5	24.4 (54)	36.56 (80)	231
			2.0	18.3 (40)	27.42 (60)	417
3	36.6 (80)	73.12 (160)	1.0	36.6 (80)	73.12 (160)	78
			1.5	24.4 (54)	48.8 (108)	171
			2.0	18.3 (40)	36.6 (80)	312
4	22.84 (50)	22.84 (50)	1.0	22.84 (50)	22.84 (50)	400
			1.5	15.23 (33)	15.23 (33)	900
			2.0	11.42 (25)	11.42 (25)	1601
5	54.84 (120)	54.84 (120)	1.0	54.84 (120)	54.84 (120)	69
			1.5	36.6 (80)	36.6 (80)	156
			2.0	27.4 (60)	27.4 (60)	278

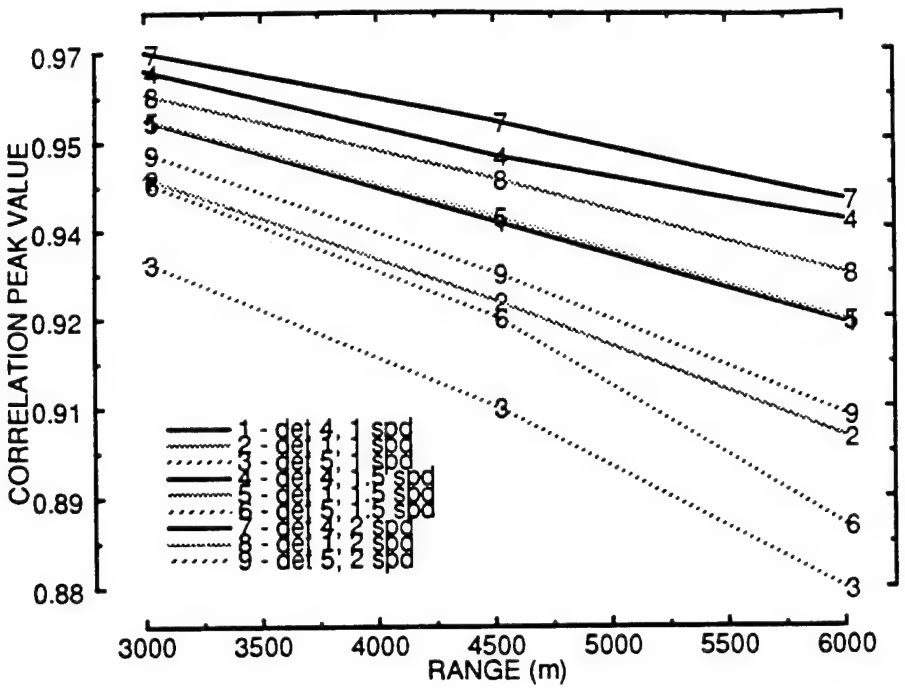

Figure 32. The influence of sampling rate variation using square detectors

Although correlation peak value may not be directly proportional to performance, one notices from the slope of the lines that a sampling rate of 1 spd produces the same correlation value as 1.5 spd at 1000 meters greater range. It is assumed that keeping the same correlation peak value for two system designs would result in equal performance of an algorithm. In going from 1.5 spd to 2.0 spd the increase in correlation value is not as great as the increase in going from 1.0 to 1.5. The correlation values for 1.5 spd are equal to those for 2.0 spd at approximately 500 meters greater range. These trends hold for the rectangular detector aspect ratios to be discussed in the next section. One would expect that for a system design in which the optics was more limiting, the influence of the detector height and sampling rate would not be as great.

5.8 SAMPLING AND DETECTOR ASPECT RATIO

It is thought by some researchers that the image quality provided by rectangular detectors is good enough for automatic target recognition applications. They point out the advantages of the improved SNR for the larger detectors as well as easier fabrication of the array. The resulting taller FOV is seen as an advantage. In this experiment we investigated the influence of detector height alone on correlation. No atmosphere was used and no noise was simulated. The detector height was changed so that its aspect ratio was 1:1 (x:y) for detector #1, 2:3 for detector #2, and 1:2 for detector #3.

The sampling rate was varied simultaneously in the x and y directions to be 1, 1.5 and 2 samples per detector subtense. Thus, if the detector height was increased for a particular sampling rate, the physical sample spacing increased, even though the sampling rate expressed as samples per

detector subtense remained constant. The increased presample filtering along with the increased sample spacing both contribute to the decreased resolution. Figure 33 illustrates the relative size of the detectors and the corresponding sampling grids.

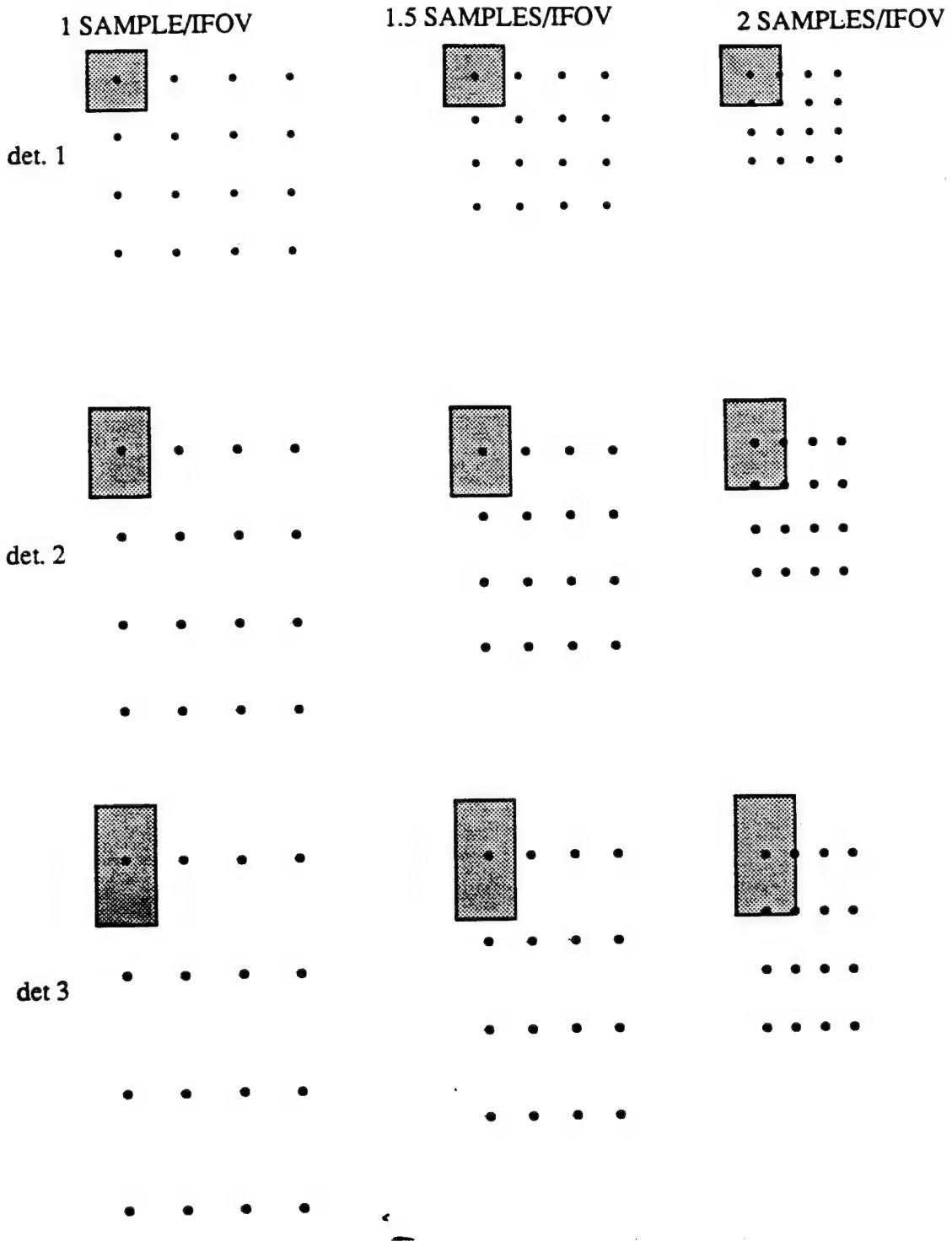

Figure 33. Relative size of detectors (shaded) and sampling grid (dots) for rectangular detectors

The curves labeled 1, 4 and 7 in Figure 34 are the same as curves 2, 5, and 8 in Figure 32 and are shown for comparison purposes. Curves 2, 5, and 8 and curves 3, 6, and 9 in Figure 32 show the results for detector 2 (aspect ratio 2:3) and detector 3 (aspect ratio 1:2) respectively. As one would expect, when the detector height increased (as the amount of prefiltering increased), the performance decreased. Also as would be expected, increasing the sampling rate improved performance in all cases.

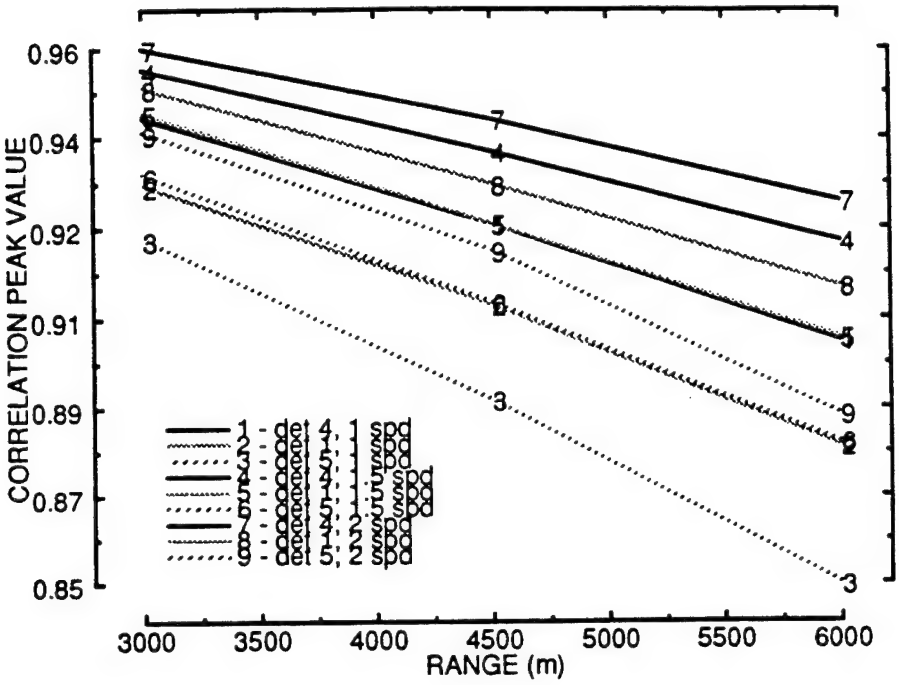

Figure 34. The influence of detector height and sample spacing

The trends for square detectors and rectangular detectors are similar. In both cases increasing the sampling rate increases the correlation. Any increase in the presample filtering, whether due to taller detectors or larger square detectors, will decrease performance. The correlation seems to be a strong function of sample density, almost independent of the number of samples per detector subtense. For evidence of this, first compare curves 2 and 6 in Figure 32 where the sample spacing is exactly the same. Curve 2 corresponds to 1 spd while curve 6 corresponds to 1.5. Curve 6 is slightly lower since the detector is larger, even though the number of spd is larger. As a second example look at curves 1, 5 and 9 in Figure 34, all of which correspond to the same sample spacing in the cross scan direction (see Figure 33). Again the curves are very close together.

If we look at the relation between sample density (in samples per mrad), forgetting about the sample rate (spd) we see in Figure 35 that correlation is a strong function of sample density, at least up to around 500 pixels per square mrad where the data starts to level off. All three sampling rates have been mixed in the graph. The data presented correspond to the 3 km case

only. The data for 4.5 and 6 km are similar and lie slightly lower in correlation than the values plotted for 3 km. This is consistent with our experience with algorithm performance being very dependent upon number of pixels on target.

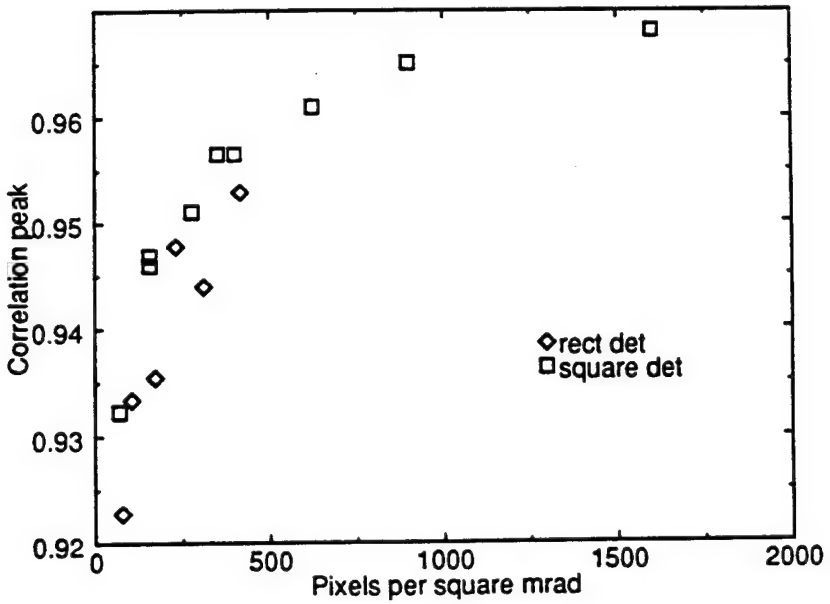

Figure 35. Correlation peak values for various pixel densities for targets at 3 km

5.9 SAMPLE-SCENE PHASE

This experiment examines the influence of the alignment of the sampling grid with the scene. The relative alignment of the sampling grid and the target has been termed sample-scene phase.[14] For an undersampled system the appearance of the target is dependent upon the sample-scene phase. The effect will not be very apparent at shorter ranges where there are several pixels on every feature of the target. However, at longer ranges where a feature is one sample wide, different alignments of the feature with the sampling grid can seriously distort the feature.

For systems which are sampled at two samples per input bandwidth, (not two samples per detector subtense unless the detector is the component which limits the bandwidth) and which are ideally reconstructed (something which never happens in present FLIRs, even in second generation systems), there should be no variation of the image with sample-scene phase. Less than ideal reconstruction can result in some sample-scene phasing effects even for a two sample per dwell system. Typical reconstruction for current FLIR systems is a sample and hold (far from ideal) or a linear interpolation (better, but not as good as could be done) in combination with a Gaussian display spot. (If the display is flat panel, the reconstruction due to the display is more like a rect function or sample and hold.) For ATRs the signal is not reconstructed but is fed directly to the signal processor, and therefore, if the FLIR has no antialiasing filter, even a system with two samples per dwell could exhibit some sample-scene phasing effects.

Simulation of small changes in the line of sight of the FLIR was accomplished by starting the sampling at different points in the reference image. Nine different sample-scene phases were tested for three different sampling rates and three different ranges, and the results are plotted in Figure 36. Data points of the same shape indicate different sample scene phases for the same sampling rate. The magnitude of the spread in correlation values for a particular sampling rate is an indication of how different a single target appears simply due to phasing.

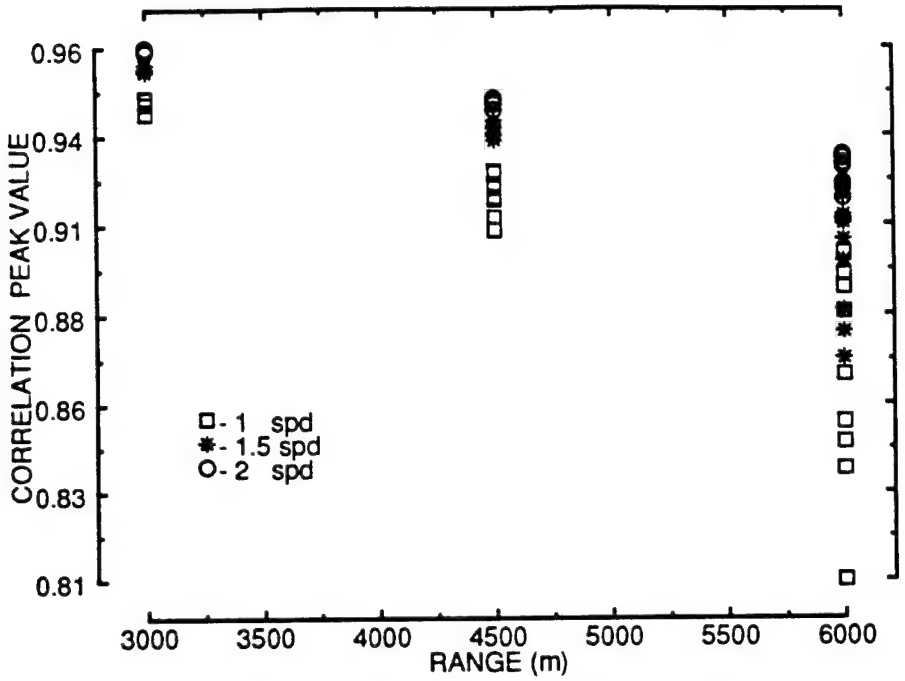

Figure 36. The influence of sample scene phasing for three different sampling rates

For a target recognizer which is trying to discriminate between several different targets, a small spread of correlation values, or ideally no spread, is desired. The larger the spread, the easier it would be for one target to appear like (have a high correlation with) another target. Thus, the spread is a measure of robustness of the system.

As one would expect, any factor which increases the size of the sampling grid relative to the target will increase the spread of correlation values due to different phases. Decreasing the sampling rate, while holding detector size constant, will increase the sampling grid spacing. Increasing the detector size, even while keeping a constant sampling rate, will increase the sampling grid spacing. Increasing the range to the target will increase the size of the sampling grid when projected onto the target.

Figure 36 shows the increasing spread of correlation values with decreased sampling rate and increased range. It is seen that at long range, the lower sampling rate results in a very large spread in correlation values.

5.10 NOISE AND DETECTOR SIZE

Figures 37 through 39 show the performance versus range for different combinations of detector size and SNR for no atmosphere, "good" atmosphere and "poor" atmosphere. For the case of no atmosphere, Figure 37, the signal in the image is very large compared with the noise, even at long range. Comparing the results for three cases (1) a small detector (detector 4) with high noise level ($\sigma = 4$ quantization levels) (2) a medium sized detector (detector 1) with a medium noise level ($\sigma = 2.5$) and (3) a large detector (detector 5) with a low noise level ($\sigma = 1.66$), one notices that for the case of no atmosphere, the degradation due to lower resolution of larger detectors dominates any degradation due to more noise of the larger detectors. This is the case at all ranges. Correlation is also plotted for detectors 1 and 5, each with the same amount of noise as is used with detector 4. This is done to get a feeling for the magnitude of benefit due only to the SNR improvement of the larger detectors.

For the good atmosphere case, Figure 38, at a range of 3000 meters the signal in the image is still much larger than the simulated noise levels and the degradation due to the poorer resolution of the larger detectors is the dominating effect. That is, the larger detectors result in lower correlation. At 4500 meters the signal in the image has been degraded to the point that the simulated noise now has significant degrading effect. The SNR benefits of going to a larger detector (detector 4 to detector 1) are being offset by the resolution penalty, resulting in the data points for the two cases overlapping. At 6000 meters the case is just opposite that at 3000 meters. The signal in the image is small enough that the improved SNR of the larger detectors provides more benefit than the improved resolution of the smaller detectors. Thus, at 6000 meters, the larger detector performs better than the smaller one. Figure 39 shows the results for the "bad" atmosphere where the SNR is so low that the larger detectors show better performance.

Whether a smaller or larger detector has a higher correlation value will depend upon the dynamic range of the input scene, the atmospheric attenuation, and several system design details including whether one can achieve BLIP. As more importance is put on longer range, degraded battlefield performance requirements, FLIR system designs will tend to favor (BLIP) systems with larger detectors. If the dominant noise source was not due to signal fluctuations the benefits of larger detectors could disappear altogether and the conclusions drawn about the optimal detector array configuration could be quite different.

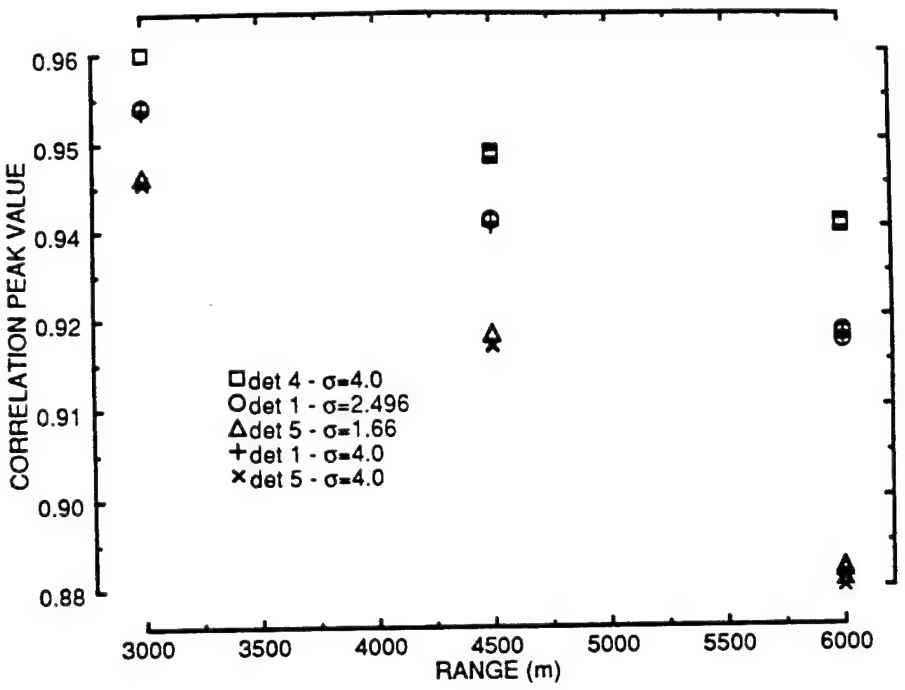

Figure 37. Correlation vs. range for different size BLIP detectors: no atmosphere

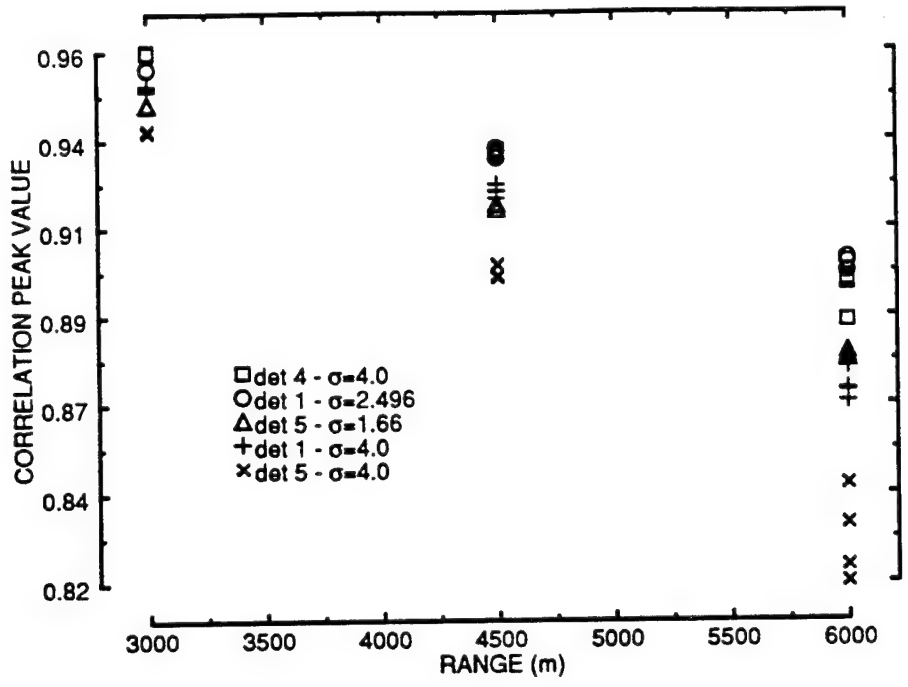

Figure 38. Correlation vs. range for different size BLIP detectors: "good" atmosphere

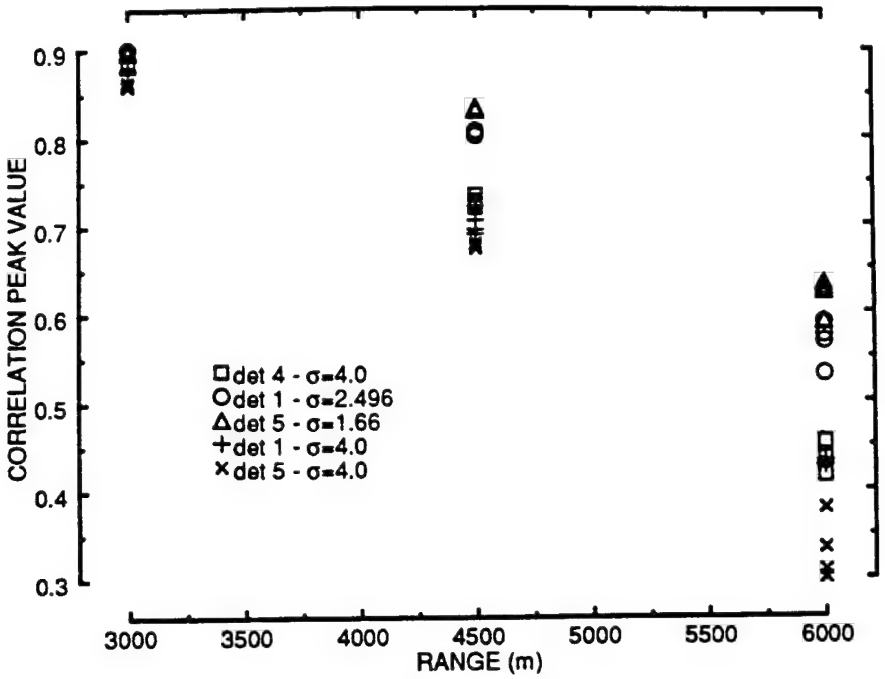

Figure 39. Correlation vs. range for different size BLIP detectors: "bad" atmosphere

5.11 RESTORATION

A complete understanding of the best image quality achievable using a particular FPA architecture can be achieved only after an investigation of the final image quality after restoration. Restoration could significantly improve the system performance for an ATR and for a human. The improvement in performance due to restoration could be used to offset the degradation in performance due to an array which was easier to build. The magnitudes of performance improvement achievable for different system designs are presently being investigated for simulated system designs and will soon be measured for real FLIR systems under an ILIR effort.

5.12 CROSS CORRELATION

Correlation values measured in the previous tests are thought to relate to the performance of future algorithms; however, efforts to link performance directly with a simple performance measure such as recognition range have met with little success. One such effort to try to translate the variation of a focal plane design parameter into range will be described.

It was thought that perhaps one could determine a range at which the correlation of a target with the degraded image of that target would be the same magnitude as the "cross correlation" of that target with another target. If the improvement in the FLIR design then resulted in separation of correlation and cross correlation values, one would have to go to longer ranges in order to have correlation and cross correlation values be equal. The difference in the two ranges would be a measure of the value of a particular improvement to the FLIR design.

In practice it was found to be very difficult to find a range at which the correlation and cross correlation were the same. The two targets used were different sizes resulting in a low cross correlation value. In order to carry out the test we would have to zoom the smaller target so that it was approximately the same size as the reference target in order to maximize the cross correlation.

Section 6 Interlace Effects on Tracking Algorithms

A second generation of ATR prototypes has been developed and third generation systems are being proposed and built. Trackers were added to second generation ATR's (an important distinction from first generation ATR's) and will be fully integrated into third generation ATR's. While second generation ATR's were proposed for stabilized platforms, the third generation ATR's will be expected to close the loop on these stabilized platforms as well as operate in more complex modes and scenarios. One of the concerns about these complex systems is the impact that a scanning sensor may have on tracking algorithm performance under motion of the platform. The interplay of the sensor, platform and tracking algorithms can best be predicted through simulation. However, this more limited analysis, which did not include simulation, does provide some insight into the negative impact of interlace misregistration on second and, by implication, third generation ATR systems.

One of the motion disturbances considered here is jitter. Jitter may be defined, for our purposes, as random wandering of the LOS about the point of interest. The main component of jitter is considered to be the residual motion remaining after stabilization of a gimbaled platform to a dominant disturbance such as the beating of the rotors of a helicopter or the vibration due to a tank's tread, etc. These "steady state" disturbances may not be the only sources of jitter, however. Sharp impulses from cannon and trains of impulses from bursts of machine guns may also be present. These disturbances may be important, depending on the scenario in which an ATR/ tracker is used. The jitter from these disturbances will exceed the stabilization specifications achieved for systems designed to suppress only the "steady state" disturbances.[15] Therefore, a worst case of two to three pixels of jitter will be assumed for a stabilized, high resolution, infrared sensor which is defined here as 2 degree FOV, 1000 x 1000 pixels.

Another motion disturbance that is considered here is that of panning for the purposes of centering a target in the FOV. Centering a target is a closed loop process that first accelerates the center of the field of view (CFOV) toward the target and then decelerates the CFOV so as to prevent the CFOV from overshooting the target. The accelerations and decelerations are on the order of 8.5 pixels/frame2. The peak velocity of the platform during the centering process is approximately 50 pixels/frame.

Two types of scanning sensors are considered with respect to the above distorting motions: bidirectional scanned and interlaced (BDSI) and uni-directional scanned and interlaced sensor systems (UDSI), as shown in Figure 2 on page 5. The BDSI sensor system, shown in Figure 40, displays a non-uniform distortion across the FOV, under a uniform motion, because the time separation between the corresponding pixels of alternate fields varies from virtually zero on the right hand side of the screen to approximately a frame time on the left hand side of the screen. It is assumed that the systems are designed so that a frame starts scanning on the left side of the FOV. Figure 41 shows the distortions of a UDSI sensor system under uniform motion. The time between corresponding pixels of the alternate fields of a this system is a field time and is constant across the FOV. The distortion under this motion would therefore be constant across the FOV for the UDSI sensor.

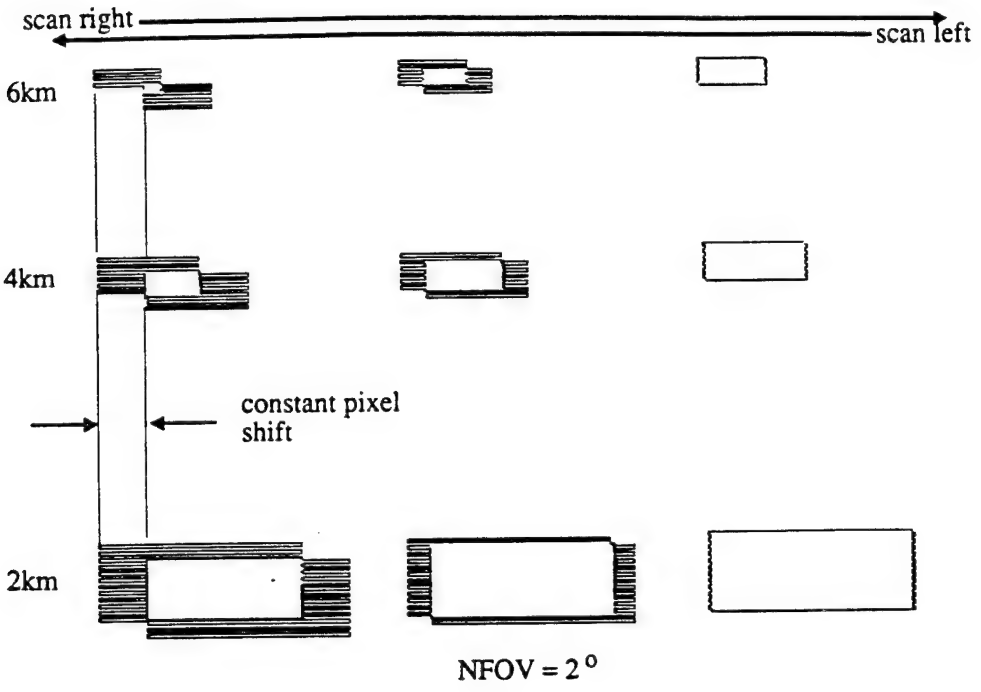

Figure 40. Target distortion of bi-directional scanning and interlaced sensor (BDSI) caused by platform motion

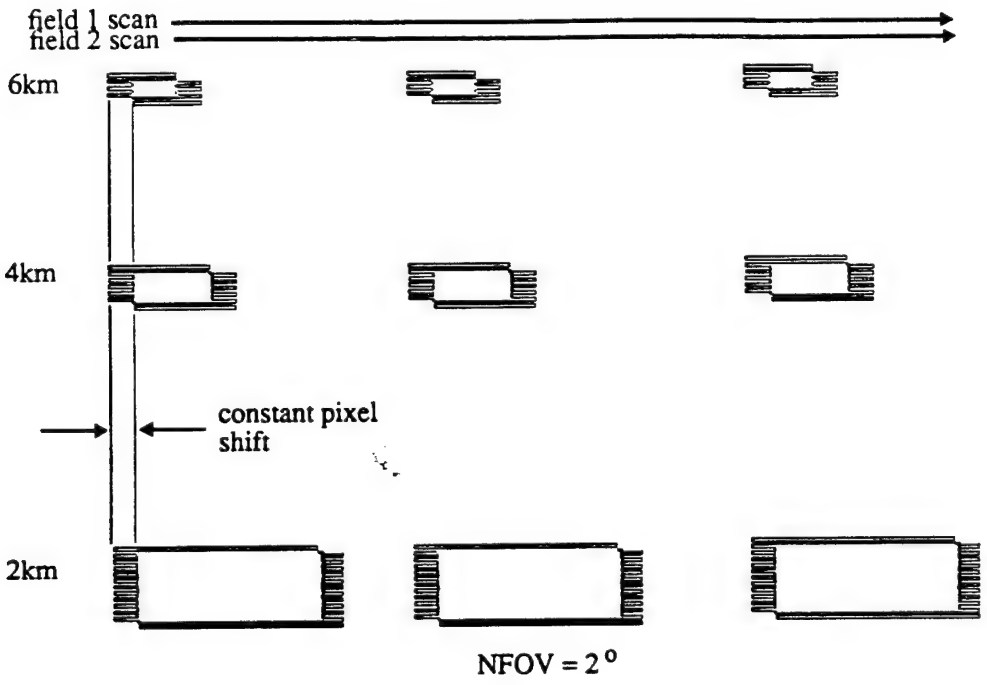

Figure 41. Target distortion of uni-directional scanning and interlaced sensor (UDSI) caused by platform motion

The basic types of trackers under consideration are the centroid tracker (CT), the correlation tracker (COR) and the predictive tracker (PT). The CT determines the center and the extent of a target in two dimensions. The CT employs a track gate which is larger than the target in order to provide an adequate margin for target and platform dynamics and errors of placement. The COR finds the relative offset for maximum correlation between a new target image (or derivative of that image) and a reference image (or derivative). The COR is limited by its offset range which is defined to be the maximum radius (in pixels) over which the full correlation of the two images is done (at each point). The limiting factor for the offset range is the throughput limitations of the COR, which increases dramatically with offset range.[15] The PT employs a CT or COR to measure the positions or relative positions of a target and then filters these measurements and makes a prediction for the next position. All of the above trackers may utilize either a single frame or single field of image data to perform their processing functions and will be referred to as either frame or field trackers.

The CT will fail if the gates are too small or badly placed so that a portion of the target consistently lies outside the target gates. The gates quickly shrink, losing the target completely. This may happen if there is not enough margin between the target and target gate to accommodate the dynamics of either the target or platform. The COR tracker may fail if the target signature varies quickly (due to obscuration etc.) thereby reducing and broadening correlation result. The COR can also fail if the offset range for correlation is exceeded by the dynamics of the platform or target. A PT will fail if its internal CT or COR fails or if its prediction is grossly in error.

6.1 EFFECTS OF JITTER

Jitter, if it is expressed as frame to frame offsets, increases the throughput requirements for the CT, COR and PT. The CT throughput requirements are increased by the expansion in the dimensions of the gate required to maintain adequate margin. The COR throughput is increased by the necessity to expand the offset range for correlation by the amount of jitter. The PT throughput is increased as the incorporated CT or COR throughput is increased. These increases in throughput requirements are similar for a BDSI, UDSI or a scanned and non-interlaced sensor. The non-interlaced sensors, however, can be expected to work as well with jitter as without since they suffer no field to field distortion.

The chief impact of field to field jitter on a frame CT is to "bias" the measurement of the centroid, as shown in Figure 42. The impact is most important at long ranges and for small targets where the aimpoint may be significantly disturbed by the "bias".

A frame COR tracker is also impacted by field to field jitter. These effects on a frame COR tracker may be computed for a binary area correlator for a three meter by three meter target (17x17 pixel front view of tank at 5Km). If there is three pixels of jitter in the horizontal direction between the reference frame and the new frame, and the segmentor removes the jagged edges (six pixels in horizontal direction) of the distorted target image, then there will be 35% loss of correlation (187 vs. 289 pixels squared or a change in target area of 102 pixels squared). A loss of this amount of correlation will typically be sufficient to place a tracker in coast mode. Even if the loss of correlation does not cause the loss of track or coasting, the uncertainty of the measurement of offset (relative target location) is directly increased by the amount of jitter, i.e.

3 pixels. This is true because the smaller resulting binary target correlates equally well within 3 pixels (horizontal). A frame COR tracker employing a non-interlaced sensor does not suffer these degradations.

An edge correlator shows the worst performance loss due to field to field jitter distortions. In Figure 42 edge correlation plots are shown for three cases, in which the new edge image has suffered no distortion, a one pixel distortion in the horizontal direction, and 2x2 pixel distortion in both dimensions. The degradation of the correlation value is obvious. It is unlikely, given normal variation about the edge of a target due to segmentation, that a reliable offset could be determined from the correlation result of the most severely distorted image. This degradation of the correlation scales up for any square target and therefore is range independent.

If a PT incorporated a COR tracker, then its predictions could be expected to suffer from the frailties of the incorporated tracker. If the uncertainties of the incorporated tracker are modeled properly then the PT may be able to improve on the offset uncertainty. However, the response to the most severe degradation of Figure 42 would be to make no prediction, i.e. coast, and possibly lose track.

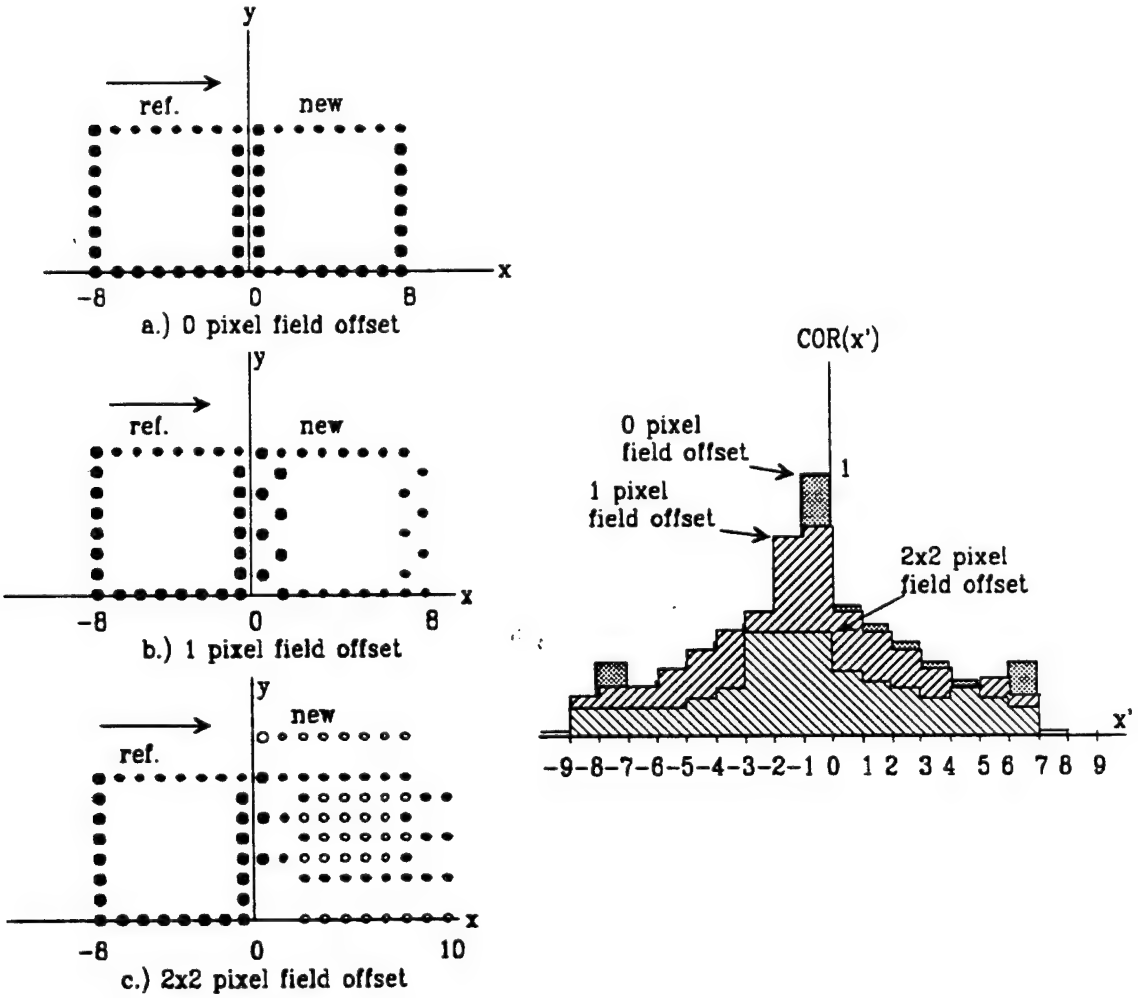

Figure 42. Binary edge correlator with field distortions

6.2 IMPACTS OF TARGET CENTERING

A panning motion of the sensor, exhibiting constant acceleration of 8 pixels per frame squared, severely impacts a CT frame tracker. The change of target image length from frame to frame (Figure 42) for a BDSI sensor (target on the left side of the FOV) is directly proportional to acceleration, i.e. eight pixels per frame. This distortion averages out the centroid between fields, i. e. four pixels ahead of the first field and four pixels behind the second field. This centroid "bias" is progressive with each frame and after three frames will be located between the separated target field images of the front view of a tank at 5km, used above. If the centroid is the aimpoint of this "target", then accurate fire is sure to miss the target. It is also unclear that both separated images will remain in the track gate. One or both of the field images may walk out of the gate before it can properly resize itself. There is a 50% chance of losing track under these circumstances. If this loss of track is to be avoided, the margin between the target and track gate must be greatly increased to handle the increased distortion of the target. For the target used above (front view of tank at 5km) the throughput requirements for the frame CT, suffering horizontal panning, would be increased by a factor of three above that required for the dynamics alone. Again these severe degradations are not present in a non-interlaced target image.

It may be argued that a ATR/tracker does not have to tell the weapon system to fire during centering. However, this is scenario dependent. It is not hard to imagine an air to air scenario in which the sensor system is constantly trying to center the target during engagement. To be unable to fire during centering would be a severe handicap.

The above panning motion presents a severe challenge for a COR frame tracker as well. An edge correlator would fail instantly. An area COR tracker, employing a BDSI sensor, could also fail instantly. Assuming jagged edges were removed by the segmentor, the correlation value for the target image used above located on the left side of the FOV would drop 50% in one frame time. In addition, there would be a 8 pixel offset uncertainty. If the jagged edges of the image were not removed by the segmentor, the peak correlation value would be reduced by 25%, and again the offset uncertainty would be increased by eight pixels. This is very poor performance and eventually the target image fields may completely separate (depending on the aspect) and cause tracking failure. Additionally, 8 pixels uncertainty increases the throughput requirements by a factor of 6 (compared to jitter). While a UDSI sensor produces half the distortion of the BDSI sensor, that is not much improvement and will only extend the operation for a few additional frames. The PT would fail if the incorporated CT and COR trackers fail.

In general then, all tracking algorithms could be expected to fail at far range during a target centering mode. This is true for both BDSI and UDSI sensors.

6.2.1 Field Trackers and Target Centering

Field trackers would seem to be an ideal solution to the distortion problems noted above. They would suffer no field offset distortion like the frame trackers that employ interlaced systems. While utilizing the same throughput, they operate at twice the speed, thereby reducing dynamics by half. However, they also have their problems. They work with a half resolution target in the vertical dimension since only a field of data is used for tracking. This may reduce maximum

range by a factor of two if the scenario requires targets to be tracked at extreme ranges or if small targets need to be tracked. In addition, a PT for a system employing a BDSI sensor will produce grossly incorrect predictions during a target centering mode due to the effective non-uniform sampling of that system. A discussion of this follows.

Assuming a very large gate, no throughput limitations and zero delay, a PT filter was designed for the apparent motion induced by the centering function. A 1/2 pixel of error was allowed for the measuring error of the incorporated CT or COR, and no jitter was assumed. In other words, this result represents the best that an in-raster PT can do. Figure 43 compares the predictive output of the PT with the calculated input position of the target image for both a UDSI and BDSI field tracker, four curves in all. The result for the UDSI sensor appears as one line indicating excellent prediction. The result for the BDSI input is not so smooth. Both curves show the target being centered after 30 fields (15 frames). The square wave acceleration and velocity are shown for reference.

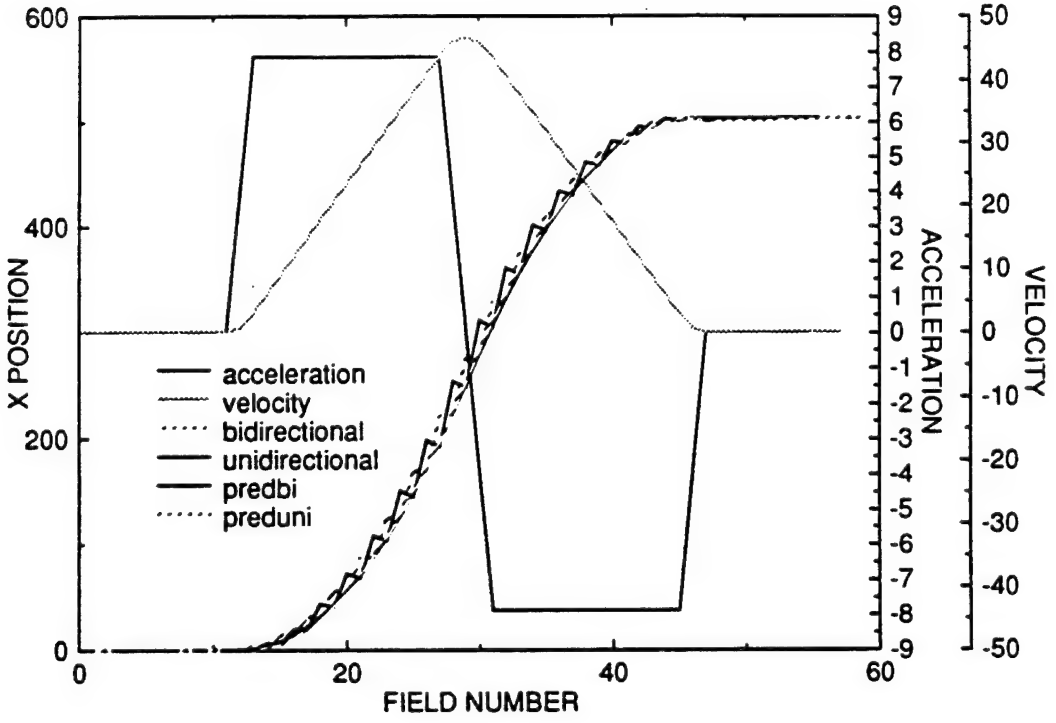

Figure 43. Predictive field tracker response to target centering - UDSI & BDSI sensor systems

The differences between the calculated and filtered results are shown more clearly in Figures 44 and 45. The predictive error for the UDSI system is less than 5 pixels, and the peaks of the error occur at the beginning and end points of the accelerations and decelerations. The peak predictive error for the BDSI sensor system is 30 pixels, and this error alternates sign with every point. Put simply: the large predictive error shown for the BDSI system is the result of the PT over-estimating and underestimating the target position from field to field. The poor prediction performance of the PT employing the BDSI sensor precludes the utilization of any field PT for this type of system.

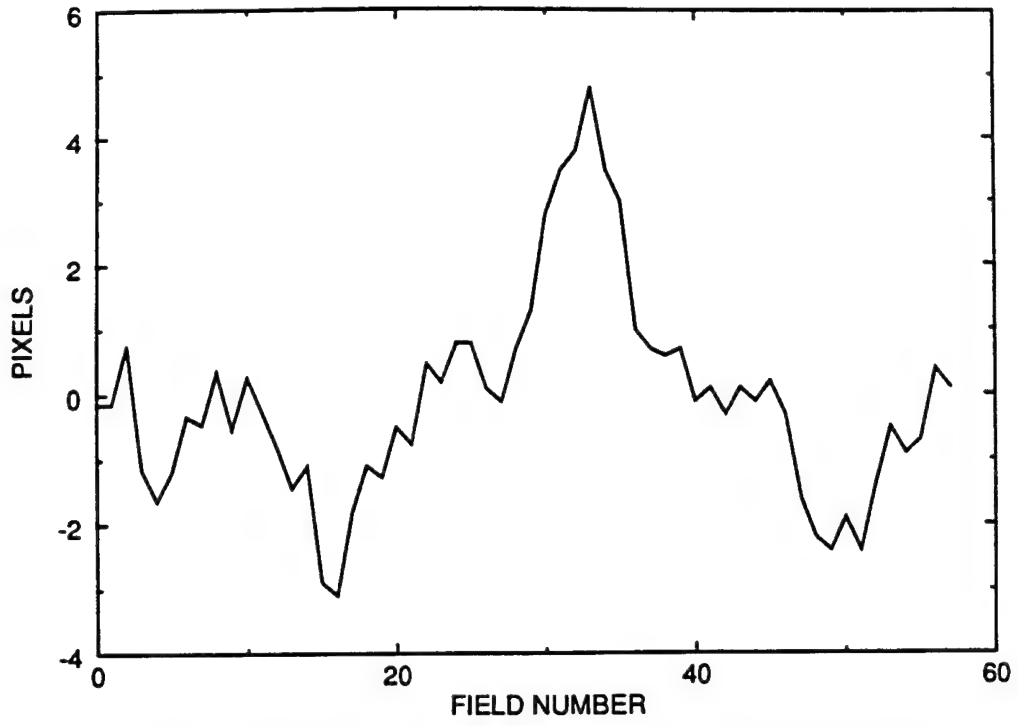

Figure 44. Difference between PT prediction and computed position for field tracker employing UDSI sensor system

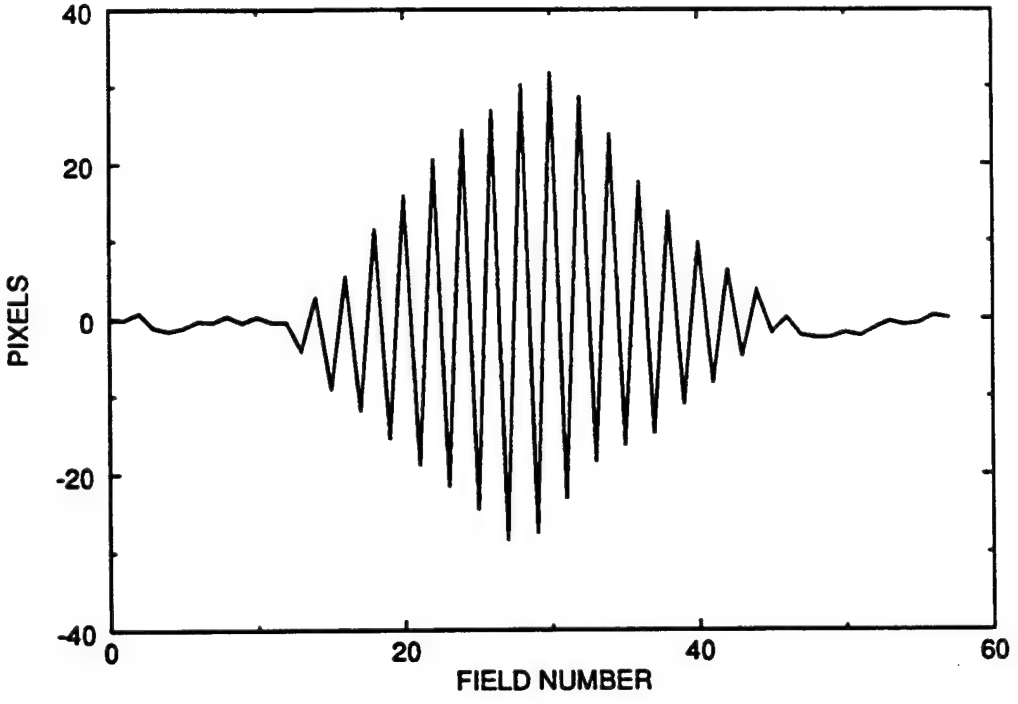

Figure 45. Difference between PT prediction and computed position for field tracker employing BDSI sensor system

6.3 TRACKER SUMMARY

In summary, it has been shown that all interlaced sensor systems present harmful image distortions to frame tracker algorithms during the sensor motions of jitter or panning. In addition, large increases of throughput are required for even marginal performance. Field trackers, though immune to most of the distortion effects, will suffer possible range limitations due to the half image height utilized by these trackers. It has also been shown that a field PT may not be employed with a BDSI sensor system if target centering is required. On the other hand, a non-interlaced sensor is not expected to present significant distortions to trackers. Throughput requirements will be increased only in direct proportion to the increased dynamics of the platform due to jitter and panning.

Therefore, for good tracking algorithm performance, the non-interlaced sensor is preferred for frame tracker algorithms. The second choice for frame tracker systems would be the UDSI sensor system, though severe problems may be anticipated during panning and centering or for highly dynamic targets such as missiles or jets. For field tracker systems, a UDSI sensor system should be employed, though a range limitation may be suffered for this system due to the half height target image of each field. The BDSI sensor should not be utilized in any tracking system (field or frame) that may experience significant jitter or relative motion such as that produced by sensor panning, platform motion, or highly dynamic targets.

Section 7 Conclusions

The influence of various infrared FPA parameters was simulated, and the correlation between the simulated image and a starting reference image was measured as an indicator of the performance of future target recognition algorithms. It has been shown that misregistration of fields of an interlaced FLIR degrades algorithm performance significantly. Various amounts of misregistration impacted the performance of several types of trackers, sometimes simply degrading performance and other times completely breaking lock. As a result of this it is recommended that imagery for ATRs and trackers be noninterlaced.

The magnitude of the performance improvement resulting from a particular FPA design change can be compared with improvements expected from other design changes by reviewing the results of the appropriate experiments. While making the comparisons it should always be kept in mind that the variables are being treated separately due to the difficulty in forming general relationships between variables which are applicable to all FPA fabrication methods, and in a real system there may be interdependencies between variables which are not reflected in this testing.

The performance of the FLIR system with varying amounts of noise and nonuniformity was a strong function of the final SNR in the image. At low SNRs (at long range or in a degraded atmosphere) correlation levels were reduced substantially. The same level of noise or nonuniformity in low SNR conditions resulted in a large spread of correlation values, a condition which would destroy the robustness of an ATR.

Large detectors destroyed the system resolution and thus the correlation values. However, if the system was assumed to be BLIP limited, larger, lower noise detectors were shown to have advantages in low SNR conditions. Increased sample density improved system performance as would be expected. Sampling the scene after prefiltering (after optics and detector spatial response) at less than two samples per input bandwidth resulted in sample-scene phase problems which led to a spread of correlation values. Less than ideal reconstruction also contributed to the phasing problem. Again, the spread of correlation values for a particular sampling geometry related to system robustness. The spread was range dependent, being very large for long ranges and low sampling rates indicating a lack of robustness of the system.

The possible benefits of image restoration should be explored further and will be in an ILIR effort.

References

1. Night Vision & Electro-Optics Directorate report, Initial Performance Evaluation of Model-Based and Template Matching Automatic Recognition Algorithms: Vol. I, Background, Methods, and Procedures, Section II, April 1992.

2. Phase I Final Report, Bandwidth Reduction and Intelligent Target Tracking (BRITT), Hughes Aircraft Co., Electro-Optical and Data Systems Group, prepared for U.S. Army Night Vision and Electro-Optics Laboratory, contract no. DAAK70-82-C-0210, June 1984.

3. Final Report, Multi-Function Target Acquisition Processor (MTAP), Hughes Aircraft Co., Electro-Optical and Data Systems Group, prepared for U.S. Army CECOM Center for Night Vision and Electro-Optics, contract no. DAAK70-82-C-0210 CDRL B001, May 1990.

4. Fukunaga, K. "Introduction to Statistical Pattern Recognition", Academic Press, pg. 72.

5. Advanced FLIR Measurements nad Analysis Concepts (AFMACI) Final Report, E. W. Arriola, Ford Aerospace, Newport Beach, CA, WRDC-TR-89-1122, 17 August 1990.

6. Advanced FLIR Measurements and Analysis Concepts, Final Report, S. S. Eucker, Boeing Military Airplanes, Wichita Kansas, August 1989, WRDC-TR-89-1087, (AD-B140 505).

7. Zegel, F. H. and Terrill, C. W., "Advanced instrumentation for calibrated IR signature acquisition and processing", KRC Symposium on Ground Vehicle Signatures, 1979.

8. J. Horger, "Image generation for perception testing using computer FLIR simulation", internal report, U.S. Army Night Vision & Electro-Optics Directorate, Ft. Belvoir, VA.

9. K. R. Castleman, Digital Image Processing, (Prentice-Hall Inc., Englewood Cliffs, 1979), pp. 260-264,.

10. J. M. Lloyd, Thermal Imaging Systems, (Plenum Press, 1975).

11. E. L. Derniak, D.G. Crowe, Optical Radiation Detectors, (John Wiley & Sons Inc., 1984).

12. Scribner, D. A., Kreuer, M. R., and Gridley, J. C., "Physical limitations to nonuniformity correction in IR focal plane arrays", Proceedings of SPIE, Vol. 865, pp. 185-202, (1985).

13. Reichenbach, S. E., and Park, S. K., "Two parameter cubic convolution for image reconstruction", Proceedings of SPIE, Vol. 1199, pp. 833-840, (1989).

14. Park, S. K. and Schowengerdt, R. A., "Image sampling, reconstruction, and the influence of sample-scene phasing", Applied Optics Vol. 21, No. 17, pp. 3142-3151 (1982).

15. "Some Effects of Platform Motion and Scanning Sensors on Tracking Algorithms", D.L. Goodwin, U.S. Army Night Vision & Electro-Optics Directorate (NVEOD), technical report (in draft), dated 20 May 1992.

16. "MTAP Target Tracking Algorithms: an Analysis", D.A. Reago, U.S. Army Night Vision & Electro-Optics Directorate (NVEOD), technical report (in draft), dated 13 Oct. 1988.

Appendix

A-1 SAMPLE EXPERIMENT FILE

In order to connect the various 'C' programs created to simulate FLIR FPA parameter changes, a system was devised to pipe the desired 'C' programs together. The main tool of this piping was an experiment file used as input to the piping system. An experiment file was written for each FPA parameter change, or combination of changes, designated as worthy of investigation in the experiment. These parameters included: samples/IFOV, detector size/shape, sample scene phasing, atmosphere, noise, and nonuniformity. Each experiment file listed all necessary 'C' programs and their required inputs in order of their usage in the piping system. The following is an example of an experiment file:

```
../image/m60_fr.ref      file containing ref image info
../image/flir11.par      file containing flir parameters
4500                     range in meters

optics                   flag for optics inputs
../image/fm60_fr.arf     input image
131.arf                  output image

sampling                 flag for sampling inputs
131.arf                  input image (after optics)
131150.arf               output image
1.5 1.5                  x sample/ifov, y sample/ifov
1 1                      # xphase, # yphase

noise                    flag for noise inputs
131150.arf               input image
1311501.arf              output image
4                        # frames
0 0                      mean & sigma for mean
1 2                      mean & sigma for variance

rescale                  flag for rescale inputs
../image/fm60_fr.arf     reference input image
1311501.arf              input image (after sampling)
131150101.arf            output image
433 347                  out sub_width,out sub_height
1                        interpolation function (bicubic)

imgshift                 flag for imgshift inputs
../image/fm60_fr.arf     reference input image
131150101.arf            input image (after rescale)
256 240                  reference image centroid
12 12                    # shifts x, # shifts y
1311501011.dat           output data file
```

Each "C" program was coded to incorporate the piping system by reading its name and necessary inputs from the experiment file during the execution of the program. Thus, by redirection, the piping system enabled programs to read any experiment file, execute the program's desired functions, and output the experiment file for the next program in the piping system to read as its input. An example of a typical command line for an experiment file would be:

optics < 1311201011.exp | sampling | noise | rescale | imgshift

where optics is the first program called, 1311201011.exp is the experiment file name, and sampling, noise, rescale, and imgshift are the subsequent programs called in that order.

The experiment file naming system was coded digitally due to a fourteen place file name limit of the Stardent computer which was used to run most of the experiment. The first ten digits in experiments with no atmosphere were coded in a specific order to indicate target, range, optics, detector, number of samples/IFOV, sample scene phasing, noise, nonuniformity, rescaling, and correlation. File names of experiments with atmosphere contained an eleventh digit to indicate the level of atmosphere added to the image. The following table is the coding chart used to create each experiment file.

1 target & aspect	2 range (m)	3 optics focal l. apert d.	4 Xdetect. Ydetect. microns	5 s/d	6 phase	7 noise	8 nonuni	9 rescale	10 X-cor	11 atm
1=m60fr	1=3000	1=0.457	1=36.6	1=1.0	0=none	0	0	1=Park	1=m60fr	sigma1
2=m60rf	2=4000	0.2032	36.6	2=2.0	1=3x3	1	1		2=m60rf	sigma2
3=bmpfr	3=4500		2=36.6	5=1.5		2	2		3=bmpfr	sigma3
4=bmprf	4=5000		54.84			3	3		4=bmprf	sigma4
	5=6000		3=36.6				4			sigma5
			73.12							sigm a6
			4=22.84							
			22.84							
			5=54.84							
			54.84							

As the processing proceeded from one program to another, each intermediate image produced was coded with an additional digit to indicate which FLIR parameter changes and/or interferences had been added to the image. For example, a three digit image name, such as 111.arf, meant that a reference image of the first target (m60front) at the closest simulated range (3000m) had only optics added to the image, whereas a seven digit image name, such as 1111511.arf, indicated that the same target, range, and optics-added image also had 1.5 samples/IFOV, sample scene phasing, and level 1 noise added to the image. This coding was necessary in order to label the intermediate images as each experiment file was read by succeeding programs in the piping system. If the intermediate images produced by each program were not labeled correctly, the next program called in the piping system would not operate on the correct image, and thus the final correlation value would be invalid. Labeling intermediate

images also decreased computer run time because parameter changes in later stages of an experiment file could be applied to an intermediate image with the required parameters previously created by another experiment file.

A-2 LIST OF ACRONYMS

ADASIM	an ADA computer language simulation of the Hughes Multifunction Target Acquisition Processor
AFMAC	Advanced FLIR Measurements and Analysis Concepts (a Wright-Patterson program)
ATR	automatic target recognizer
BDSI	I-directional scanned and interlaced
CFOV	center field of view
COR	correlation tracker
CT	centroid tracker
F/#	F Number - speed of lens - length/diameter of optic aperture
FFT	fast Fourier transform
FLIR	forward looking infrared system
FOV	field of view
FPA	focal plane array
IFOV	instantaneous field of view - detector angular subtense
ILIR	independent lab in-house research
IR	infrared
IRFPA	infrared focal plane array
LOS	line of sight
MTF	modulation transfer function
NET	noise equivalent temperature (difference)
PT	predictive tracker
SNR	signal to noise ratio
SPD	samples per dwell
UDSI	uni-directional scanned and interlaced

Distribution for Report No. AMSEL-NV-TR-0118

20 Director
US Army CECOM
Night Vision and Electronic Sensors Directorate
ATTN: AMSEL-RD-NV-V
10221 Burbeck Road
Fort Belvoir, VA 22060-5806

1 Director
US Army Communications Electronics Command
ATTN: AMSEL-RD-D
Fort Monmouth, NJ 07703-5000

1 Director
US Army Materiel Systems Analysis Activity
ATTN: AMXSY-D
APG, MD 21005-5071

2 Defense Technical Information Center
ATTN: DTIC-FDA
Cameron Station, Bldg. 5
5010 Duke Street
Alexandria, VA 22304

2 Director
US Army TRADOC Analysis Center
ATTN: ATRC-W
White Sands Missile Range, NM 88002-5502

2 Project Manager
Night Vision Devices
US Army Center for Night Vision and Electro-Optics
Fort Belvoir, VA 22060-5806

2 Director
Advanced Research Projects Agency (ARPA)
3701 N. Fairfax Drive
Arlington, VA 22203-1714